

Scrutinizing LSP Dark Matter at the LHC

Manuel Drees^a, Yeong Gyun Kim^b, Mihoko M. Nojiri^b,

Daisuke Toya^c, Kazumi Hasuko^c and Tomio Kobayashi^c

^a *Physik Department, TU München, D-85748 Garching, Germany*

^b *YITP, Kyoto University, Kyoto, 606-8502, Japan*

^c *ICEPP, University of Tokyo, Hongo, Bunkyo, Tokyo, 113-0033, Japan*

Abstract

We show that LHC experiments might well be able to determine all the parameters required for a prediction of the present density of thermal LSP relics from the Big Bang era. If the LSP is an almost pure bino we usually only need to determine its mass and the mass of the $SU(2)$ singlet sleptons. This information can be obtained by reconstructing the cascade $\tilde{q}_L \rightarrow \tilde{\chi}_2^0 q \rightarrow \tilde{\ell}_R \ell q \rightarrow \tilde{\chi}_1^0 \ell^+ \ell^- q$. The only requirement is that $m_{\tilde{\ell}_R} < m_{\tilde{\chi}_2^0}$, which is true for most of the cosmologically interesting parameter space. If the LSP has a significant higgsino component, its predicted thermal relic density is smaller than for an equal-mass bino. We show that in this case squark decays also produce significant numbers of $\tilde{\chi}_4^0$ and $\tilde{\chi}_2^\pm$. Reconstructing the corresponding decay cascades then allows to determine the higgsino component of the LSP.

1 Introduction

The Minimal Supersymmetric Standard Model (MSSM) [1] is one of the most promising extensions of the Standard Model. It offers a natural solution of the hierarchy problem [2], amazing gauge coupling unification [3], and Dark Matter candidates [4]. If Nature chooses low energy supersymmetry (SUSY), sparticles will be found *for sure*, as they will be copiously produced at future colliders such as the Large Hadron Collider (LHC) at CERN or TeV scale e^+e^- linear colliders (LC). The LHC would be a great discovery machine if SUSY breaking masses lie below a few TeV [5]. On the other hand, there are several on-going and future projects searching for LSP Dark Matter. One of them even claims a positive signal [6], although the current situation is rather contradictory [7]. In any case, it seems very plausible that both SUSY collider signals and LSP Dark Matter in the Universe will be found in future.

Recently interesting possibilities have been pointed out where non-thermal production of Dark Matter is significant [8, 9]. Generally the known bound from the thermal LSP density may easily be evaded by assuming a low post-inflationary reheating temperature of the Universe, without endangering the standard successes of Big Bang cosmology [10]. If the reheating temperature is below the neutralino decoupling temperature, the relation between neutralino pair annihilation rates and the mass density of the Universe disappears. The mass may then be determined by other parameters, such as the Q ball formation rate and decay time [9], or the moduli masses and their decay rates to LSPs [8].

While these non-thermal mechanisms open exciting new possibilities, direct experimental or observational tests of them might be difficult, since they all have to occur before Big Bang nucleosynthesis (BBN).¹ It is therefore interesting to determine

1. the actual LSP relic density, both “locally” (in the solar system) and averaged over the Universe; and
2. the predicted thermal LSP relic density,

as precisely as possible. These quantities are closely related to the mass and interactions of the LSP. A positive difference between the actual and predicted LSP density would indicate the existence of non-thermal relics, whereas a negative difference would hint at large entropy production below the LSP freeze-out temperature (e.g. due to a low reheating temperature).

The matter density in the Universe divided by the critical density, Ω_{matter} , is claimed to be tightly constrained already; $\Omega_{\text{matter}} = 0.35 \pm 0.07$ [12]. On the other hand, the thermal relic density of the Universe $\Omega_{\tilde{\chi}_1^0} h^2$ ($h = 0.65 \pm 0.05$) has been calculated through the mass and interaction of the LSP, which is likely to be the lightest neutralino $\tilde{\chi}_1^0$. In the absence of direct production of sparticles we have to rely on experimental lower bounds on sparticle masses as well as naturalness arguments to conclude that the predicted $\Omega_{\tilde{\chi}_1^0} h^2$ lies somewhere between 10^{-3} and 10^3 ; clearly this is not a very useful prediction, although it is encouraging that this wide range at least includes the correct value. The purpose of this paper is to discuss how future LHC experiments can contribute to the determination of the MSSM parameters that are needed to predict the thermal LSP relic density and the LSP-nucleon scattering cross section. Our goal is thus somewhat different from that of ref.[13], where it was simply assumed that all relevant parameters had somehow been determined by various experiments, with given errors; the main emphasis was on estimating the resulting uncertainties in the predictions of the thermal LSP relic density and the LSP-nucleon scattering cross section. In contrast, we discuss in some detail *how* these parameters can be determined, and with what errors.

¹For the Q ball case, measurements of the cosmic microwave background by the MAP and PLANCK satellites might find isocurvature fluctuations due to the Affleck-Dine Field [11].

The determination of mass parameters has been discussed in detail in the minimal supergravity (mSUGRA) model, where one assumes universality of scalar masses and of gaugino masses at the scale M_X of Grand Unification [14]. In Sec. 2, we point out that $\tilde{\chi}_2^0 \rightarrow \tilde{e}_R$ is open for most parameters giving a reasonable LSP density, making the determination of $m_{\tilde{\chi}_2^0}$, $m_{\tilde{\chi}_1^0}$ and $m_{\tilde{e}_R}$ possible at the LHC. We demonstrate that the mass density is determined by the LSP and slepton masses, if the LSP is mostly a bino as expected in mSUGRA. In this case $\Omega_{\tilde{\chi}_1^0}$ can be predicted to about 10 to 20% accuracy.

In Secs. 3 and 4 we discuss a non-mSUGRA scenario. In Sec. 3 we relax the assumption of universal scalar masses for Higgs bosons. It is then easy to find cases with comparable higgsino and gaugino masses, $\mu \sim M$, while keeping all squared scalar masses positive at M_X . The LSP then has a significant higgsino component, so that its density cannot be predicted by only studying $\tilde{\chi}_2^0 \rightarrow \tilde{e}_R \rightarrow \tilde{\chi}_1^0$ decays. The situation is further complicated if we also relax the assumption of universal gaugino masses, since the neutralino mass matrix then depends on three independent, unknown mass parameters. We point out that the cascade decay $\tilde{\chi}_2^+ \rightarrow \tilde{\nu}_L \rightarrow \tilde{\chi}_1^+$ can then often be identified, providing clear evidence that $\mu \sim M$. In Sec. 4 we present a detailed case study with $\mu \sim M_2$ to confirm the potential of LHC experiments to analyze $\tilde{\chi}_2^+$ cascade decays; this allows a complete determination of the neutralino mass matrix (in the absence of CP-violating phases). Sec. 5 is devoted to discussions.

2 $\Omega_{\tilde{\chi}_1^0}$ in mSUGRA

In the minimal supergravity model one assumes universal soft breaking parameters at the GUT scale: a universal scalar mass m , universal gaugino mass M , universal trilinear coupling A , and Higgs mass parameter B . The renormalization group evolution of soft breaking squared Higgs masses then leads to consistent breaking of the electroweak symmetry, provided the higgsino mass parameter μ can be tuned independently. In this paper, we chose the weak scale input parameters $m_b(m_b) = 4.2$ GeV, $m_t(m_t) = 165$ GeV, and $\tan\beta$. We minimize the tree level potential at renormalization scale $Q = \sqrt{m_t m_b}$, which reproduces the correct value of μ obtained by minimizing the full 1-loop effective potential. We include loop corrections to the masses of neutral Higgs bosons, including leading two-loop corrections [15].

The mass density $\Omega_{\tilde{\chi}_1^0} h^2$ of the LSP is calculated from the pair annihilation cross section by using the expressions [16]

$$\begin{aligned} \Omega_{\tilde{\chi}_1^0} h^2 &= \frac{1.07 \times 10^9 / \text{GeV} x_F}{\sqrt{g_*} M_P (a + 3b/x_F)} \\ \sigma(\tilde{\chi}_1^0 \tilde{\chi}_1^0 \rightarrow \text{all}) v &= a + bv^2 \\ x_F (\equiv m_{\tilde{\chi}_1^0} / T_F) &= \log \frac{(0.764 M_P (a + 6b/x_F) c(2 + c) m_{\tilde{\chi}_1^0})}{\sqrt{g_*} x_F} \end{aligned} \quad (1)$$

except near regions of parameter space where special care is needed. Here $M_P = 1.22 \cdot 10^{19}$ GeV is the Planck mass, and a and b are the first two coefficients in the Taylor expansion of the pair annihilation cross section of the LSP with respect to the relative velocity v of the LSP pair in its center of mass frame. g^* is the effective number of relativistic degrees of freedom at LSP freeze-out temperature T_F . The expansion in v breaks down around s -channel poles; here the thermal average is calculated numerically, using the formalism given by Griest and Seckel [17]. We also take into account sub-threshold annihilation into hh and W^+W^- final states. When the LSP is higgsino-like, coannihilation of $\tilde{\chi}_1^0$ with $\tilde{\chi}_1^+$ and $\tilde{\chi}_2^0$ are important [18, 19].

The annihilation modes $\tilde{\chi}_1^0 \tilde{\chi}_1^+ \rightarrow ff'$ and $\tilde{\chi}_1^0 \tilde{\chi}_2^0 \rightarrow f\bar{f}$ are approximated by s -channel W and Z exchange, respectively; $\tilde{\chi}_1^0 \tilde{\chi}_1^+ \rightarrow W\gamma$ is also included. All other higgsino coannihilation modes are treated assuming $SU(2)$ invariance. We also include one loop radiative corrections to the mass splitting of higgsino-like states [20]. We do not include $\tilde{\chi}_1^0 \tilde{\tau}$ coannihilation, since we do not study cases with $m_{\tilde{\chi}_1^0} \simeq m_{\tilde{\tau}}$.

MSUGRA predicts a bino-like LSP $\tilde{\chi}_1^0$ and wino-like $\tilde{\chi}_1^+$ and $\tilde{\chi}_2^0$ for moderate values of m and M (below ~ 500 GeV). This is a rather model independent result [21]. Large positive corrections to squark masses from gaugino loops, together with the large top Yukawa coupling, drive the squared soft breaking Higgs mass m_2^2 negative at the weak scale. On the other hand, correct symmetry breaking requires $m_2^2 + \mu^2 > -m_Z^2/2$. One has to make μ large to obtain the correct electroweak symmetry breaking scale, if scalar masses and gaugino masses are of the same order.

If slepton masses are moderate, the LSP is bino-like, and one is sufficiently far away from s -channel poles ($2m_{\tilde{\chi}_1^0} \neq m_Z, m_{\text{Higgs}}$), the mass density is essentially determined by t -channel \tilde{e}_R exchange [19]. This is because

1. A pure bino couples only to fermion and sfermion, or Higgs and higgsino. Higgsino exchange is suppressed for $\mu^2 \gg M^2$.
2. $m_{\tilde{e}_R} < m_{\tilde{e}_L} \simeq m_{\tilde{\nu}} \ll m_{\tilde{q}}$ in mSUGRA, therefore \tilde{e}_R exchange is least suppressed by large masses in the propagator.
3. The hypercharges of sleptons satisfy the relation $Y_{\tilde{e}_R} = 2Y_{\tilde{e}_L}$, therefore $\sigma(\tilde{e}_R)v = 16\sigma(\tilde{e}_L \text{ or } \tilde{\nu}_L)v$ when sfermion masses are equal.

This can be seen in Fig. 1 a)-d), where $\Omega_{\tilde{\chi}_1^0}$ (a, b) and $b \equiv 10^6 \text{ GeV}^2 \times \Omega_{\tilde{\chi}_1^0} h^2 \sigma_{\tilde{B}}$ (c,d) are plotted. Here $\sigma_{\tilde{B}}$ is the scaled bino pair annihilation cross section in the limit where $m_{\tilde{e}_R} \ll m_{\tilde{e}_L}, m_{\tilde{q}}$ [19],

$$\sigma_{\tilde{B}} = \frac{m_{\tilde{\chi}_1^0}^2}{(m_{\tilde{e}_R}^2 + m_{\tilde{\chi}_1^0}^2)^2} \times \left[\left(1 - \frac{m_{\tilde{\chi}_1^0}^2}{m_{\tilde{e}_R}^2 + m_{\tilde{\chi}_1^0}^2} \right)^2 + \frac{m_{\tilde{\chi}_1^0}^4}{(m_{\tilde{e}_R}^2 + m_{\tilde{\chi}_1^0}^2)^2} \right]. \quad (2)$$

We find that the mass density increases with increasing $M \propto m_{\tilde{\chi}_1^0}$ and m ; m is essentially proportional to $m_{\tilde{e}_R}$ for $m \geq M$. Dotted lines are for constant $\tilde{\chi}_1^0$ mass. The fact that it basically only depends on M indicates that the LSP is indeed bino-like. The mass density becomes very small for $m_{\tilde{\chi}_1^0} = m_Z/2$, because LSP pair annihilation through Z exchange is enhanced. In Fig. 1 c) and 1d) we show contours of constant b . Although $\Omega_{\tilde{\chi}_1^0} h^2$ changes by more than a factor of 4, the change of b is very small over the wide range of parameter region with $M > 160$ GeV, again confirming the bino-like nature of the LSP for the mSUGRA case.

The $\tan\beta$ dependence is also very weak, as can be seen in Fig. 2 a) and b). This again shows that the LSP is bino dominant, and bino-higgsino mixing, which is controlled by the off-diagonal elements of the neutralino mass matrix, has negligible effect on the LSP relic density for the parameters given in the plot. For sufficiently heavy $\tilde{\chi}_1^0$, $\Omega_{\tilde{\chi}_1^0}$ is simply determined by $m_{\tilde{e}_R}$ and $m_{\tilde{\chi}_1^0}$ so that $b \sim 1$.

We now show that analyses of sparticle production at the LHC would lead to tight constraints on the predicted thermal relic density $\Omega_{\tilde{\chi}_1^0} h^2$. Recently, quite a few studies of precision measurements of sparticle masses at the LHC have been performed. When the cascade decay $\tilde{q} \rightarrow \tilde{\chi}_2^0 \rightarrow \tilde{e}_R \rightarrow \tilde{\chi}_1^0$ is open, a clean SUSY signal is $ll + jets + \text{missing } E_T$. It was shown [14] that $m_{\tilde{q}}, m_{\tilde{\chi}_2^0}, m_{\tilde{e}_R}$ and $m_{\tilde{\chi}_1^0}$ can be reconstructed from the upper end points of the m_{jll} and m_{jl}

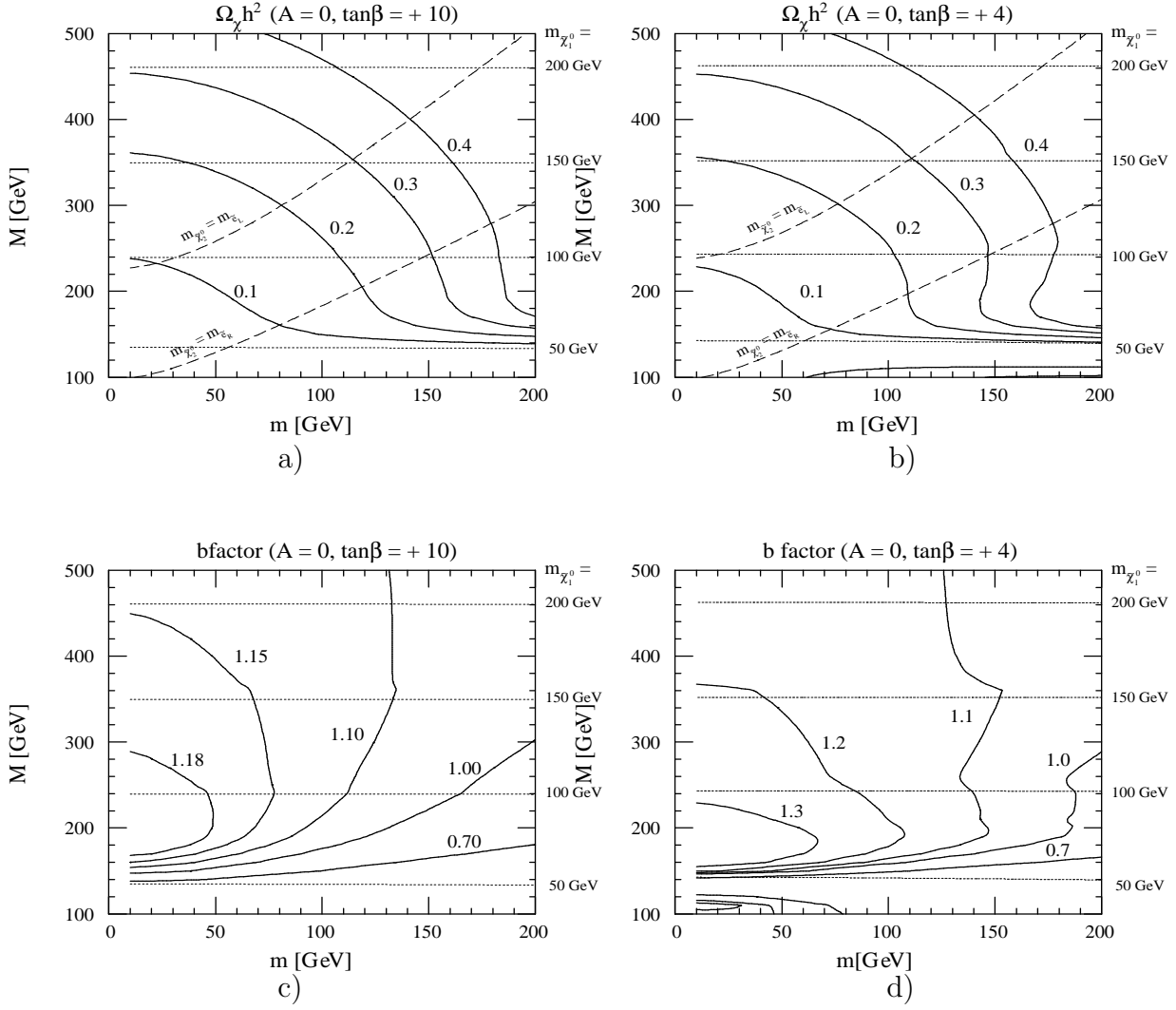


Figure 1: Contours of constant $\Omega_{\tilde{\chi}_1^0} h^2$ (Fig 1 a,b) and b factor (Fig 1 c,d) in the (m, M) plane for $\tan\beta = 10$ (a,c) and 4 (b,d). We take $\mu > 0$. Contours of constant $m_{\tilde{\chi}_1^0}$, as well as contours where $m_{\tilde{\chi}_1^0} = m_{\tilde{e}_R}$ and $m_{\tilde{\chi}_1^0} = m_{\tilde{e}_L}$ are also shown.

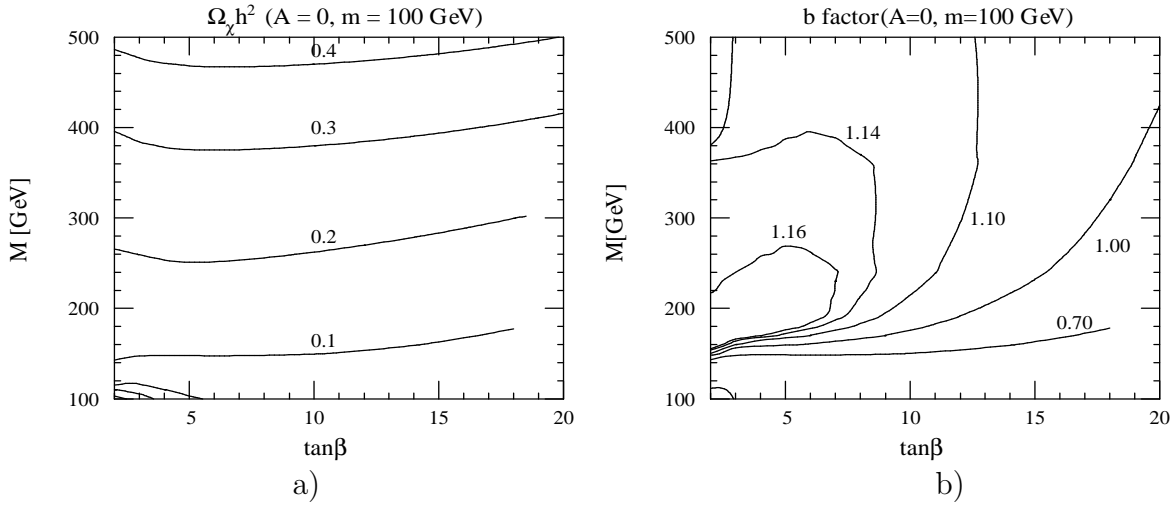


Figure 2: $\Omega_{\tilde{\chi}_1^0} h^2$ and the b factor in the $(\tan\beta, M)$ plane for fixed m .

distributions, m_{jl}^{\max} and m_{jl}^{\min} ; the edge of the m_{ll} distribution, m_{ll}^{\max} ; and the lower end point of the m_{jl} distribution with $m_{ll} > m_{ll}^{\max}/\sqrt{2}$, m_{jl}^{\min} . Here j refers to one of the two hardest jets in the event. In most cases it is chosen such that it has the smaller jll invariant mass; this is meant to select the jet from the primary $\tilde{q} \rightarrow \tilde{\chi}_2^0 q$ decay. However, m_{jl}^{\min} is reconstructed by taking the jet which gives the larger jll invariant mass, in order to avoid contamination. Those end points are given by the analytical formulae [14]:

$$\begin{aligned}
m_{jl}^{\max} &= \left[\frac{(m_{\tilde{q}L}^2 - m_{\tilde{\chi}_2^0}^2)(m_{\tilde{\chi}_2^0}^2 - m_{\tilde{\chi}_1^0}^2)}{m_{\tilde{\chi}_2^0}^2} \right]^{1/2} \\
m_{jl}^{\max} &= \text{Max} \left(\left[\frac{(m_{\tilde{q}L}^2 - m_{\tilde{\chi}_2^0}^2)(m_{\tilde{\chi}_2^0}^2 - m_{\tilde{e}_R}^2)}{m_{\tilde{\chi}_2^0}^2} \right]^{1/2}, \left[\frac{(m_{\tilde{q}L}^2 - m_{\tilde{\chi}_2^0}^2)(m_{\tilde{e}_R}^2 - m_{\tilde{\chi}_1^0}^2)}{m_{\tilde{e}_R}^2} \right]^{1/2} \right) \\
m_{ll}^{\max} &= \sqrt{\frac{(m_{\tilde{\chi}_2^0}^2 - m_{\tilde{e}_R}^2)(m_{\tilde{e}_R}^2 - m_{\tilde{\chi}_1^0}^2)}{m_{\tilde{e}_R}^2}} \\
m_{jl}^{\min} &= \frac{1}{4m_{\tilde{\chi}_2^0}^2 m_{\tilde{e}_R}^2} \left[-m_{\tilde{\chi}_1^0}^2 m_{\tilde{\chi}_2^0}^4 + 3m_{\tilde{\chi}_1^0}^2 m_{\tilde{\chi}_2^0}^2 m_{\tilde{e}_R}^2 - m_{\tilde{\chi}_2^0}^4 m_{\tilde{e}_R}^2 - m_{\tilde{\chi}_2^0}^2 m_{\tilde{e}_R}^4 - m_{\tilde{\chi}_1^0}^2 m_{\tilde{\chi}_2^0}^2 m_{\tilde{q}L}^2 \right. \\
&\quad \left. - m_{\tilde{\chi}_1^0}^2 m_{\tilde{e}_R}^2 m_{\tilde{q}L}^2 + 3m_{\tilde{\chi}_2^0}^2 m_{\tilde{e}_R}^2 m_{\tilde{q}L}^2 - m_{\tilde{e}_R}^4 m_{\tilde{q}L}^2 + (m_{\tilde{\chi}_2^0}^2 - m_{\tilde{q}L}^2) \times \right. \\
&\quad \left. \sqrt{(m_{\tilde{\chi}_1^0}^4 + m_{\tilde{e}_R}^4)(m_{\tilde{\chi}_2^0}^2 + m_{\tilde{e}_R}^2)^2 + 2m_{\tilde{\chi}_1^0}^2 m_{\tilde{e}_R}^2 (m_{\tilde{\chi}_2^0}^4 - 6m_{\tilde{\chi}_2^0}^2 m_{\tilde{e}_R}^2 + m_{\tilde{e}_R}^4)} \right] \quad (3)
\end{aligned}$$

In addition to those quantities, one can measure the end point m_{jl}^{\min} of the distribution of the smaller of the two m_{jl} values. It can be expressed as

$$\begin{aligned}
m_{jl}^{\min} &= \sqrt{\frac{(m_{\tilde{q}L}^2 - m_{\tilde{\chi}_2^0}^2)(m_{\tilde{e}_R}^2 - m_{\tilde{\chi}_1^0}^2)}{2m_{\tilde{e}_R}^2 - m_{\tilde{\chi}_1^0}^2}} \quad \text{if } 2m_{\tilde{e}_R}^2 - (m_{\tilde{\chi}_1^0}^2 + m_{\tilde{\chi}_2^0}^2) < 0 \\
&= \sqrt{\frac{(m_{\tilde{q}L}^2 - m_{\tilde{\chi}_2^0}^2)(m_{\tilde{\chi}_2^0}^2 - m_{\tilde{e}_R}^2)}{m_{\tilde{\chi}_2^0}^2}} \quad \text{if } 2m_{\tilde{e}_R}^2 - (m_{\tilde{\chi}_1^0}^2 + m_{\tilde{\chi}_2^0}^2) > 0 \quad (4)
\end{aligned}$$

Because there are only four masses involved, the last end point is redundant, but might be useful to cross check the decay kinematics.²

For the example studied in [14], the so-called “point 5”, $m = 100$ GeV and $M = 300$ GeV, which results in $m_{\tilde{\chi}_2^0} = 233$ GeV, $m_{\tilde{e}_R} = 157.2$ GeV and $m_{\tilde{\chi}_1^0} = 121.5$ GeV. The errors on $m_{\tilde{e}_R}$ and $m_{\tilde{\chi}_1^0}$ are strongly correlated and are found to be 12% for $m_{\tilde{\chi}_1^0}$ and 9% for $m_{\tilde{e}_R}$. Within the framework of mSUGRA the measured LSP mass excludes the possibility that s -channel poles are important for the LSP pair annihilation cross section (see below). We find that the corresponding error on $\sigma_{\tilde{B}}$, and hence on the prediction for $\Omega_{\tilde{\chi}_1^0} h^2$, for this parameter point is 20%. If the error (which is dominated by systematics associated with uncertainties of signal distributions) is reduced by a detailed study of various signal distributions, the error on $\sigma_{\tilde{B}}$ may go down below 10%.

²We are assuming that squarks are basically degenerate. Note that essentially only left-handed squarks will contribute here, since $SU(2)$ singlet squarks very rarely decay into $\tilde{\chi}_2^0$. Barring “accidental” cancellations, bounds on flavor changing neutral current processes imply that squarks with equal gauge quantum numbers must be close in mass. The mass splitting between \tilde{u}_L and \tilde{d}_L squarks is limited by $SU(2)$ invariance. With the possible exception of third generation squarks the assumed degeneracy therefore holds almost model-independently. If required, contributions from third generation squarks can be filtered out by anti-tagging b -jets.

Fig. 1 also contains contours where $m_{\tilde{\chi}_2^0} = m_{\tilde{e}_R}$ and $m_{\tilde{\chi}_2^0} = m_{\tilde{e}_L}$. To the left of these contours $\tilde{\chi}_2^0$ decays into \tilde{l} are accessible, giving a substantial constraint to the kinematics of the events. First, note that $\tilde{\chi}_2^0 \rightarrow \tilde{e}_R$ decays are open for most of the cosmologically acceptable region with $M \geq 200$ GeV. There is even a substantial region of parameter space where both $\tilde{\chi}_2^0 \rightarrow \tilde{e}_L$ and $\tilde{\chi}_2^0 \rightarrow \tilde{e}_R$ are open. In our argument above, we assumed that all observed edges and end points kinematic distributions come from $\tilde{q}_L \rightarrow \tilde{\chi}_2^0 \rightarrow \tilde{e}_R$ rather than $\tilde{\chi}_2^0 \rightarrow \tilde{e}_L$. When the latter decay mode is open, the branching ratio dominates over \tilde{e}_R , since $\tilde{\chi}_2^0 \simeq \tilde{W}_3$ and \tilde{e}_R is an $SU(2)$ singlet. However if one assumes that squared scalar masses are positive at the GUT scale, \tilde{e}_L cannot be too much lighter than $\tilde{\chi}_2^0$, so there is some kinematical suppression. In mSUGRA the relevant masses are expressed as:

$$\begin{aligned} M_1 &= 0.4M, & M_2 &= 0.8M \\ m_{\tilde{e}_L}^2 &= m^2 + 0.5M^2 - \left(\frac{1}{2} - \sin^2 \theta_W\right) m_Z^2 \cos 2\beta \\ m_{\tilde{e}_R}^2 &= m^2 + 0.15M^2 - \sin^2 \theta_W m_Z^2 \cos 2\beta, \end{aligned} \quad (5)$$

and $m_{\tilde{\chi}_1^0} \sim M_1$ and $m_{\tilde{\chi}_2^0} \sim M_2$ if $M \ll \mu$. In [14], it was shown that the two edges can be observed separately even if $\tilde{\chi}_2^0 \rightarrow \tilde{e}_L$ is not strongly phase space suppressed. It might also be possible to find evidence for light left-handed sleptons by looking into the relative strengths of different SUSY signals. If $\tilde{\chi}_2^0 \rightarrow \tilde{e}_L, \tilde{\nu}_L$ is open, $\tilde{\chi}_1^+ \rightarrow \tilde{e}_L$ or $\tilde{\nu}_L$ is also open and dominant, yielding relatively large $l^+ l'^-$ and $l^+ l^- l'$ signals compared to the $l^+ l^-$ signal.

If we assume bottom Yukawa corrections are negligible and squared scalar masses are positive at the GUT scale, the pseudoscalar Higgs mass m_A is bounded from below as $m_A^2 > \mu^2 + m_{\tilde{\nu}}^2$ [22]. Under the bino dominant assumption, and for moderate value of $\tan \beta$, neutralino annihilation through s -channel poles can thus not be important. On the other hand, for large $\tan \beta$ the pseudoscalar Higgs boson can be light enough to achieve $m_{\tilde{\chi}_1^0} \sim m_A/2$ [22, 19]. However, in mSUGRA large $\tan \beta$ also implies a rather light $\tilde{\tau}_1$, which greatly depletes the $l^+ l^-$ signal [23]; the observation of strong multi-lepton signals would thus already indicate that $\tan \beta$ is not very large. Note also that for large $\tan \beta$ direct production of the heavy neutral Higgs bosons from gluon fusion and/or in association with $b\bar{b}$ pairs allows to detect or exclude these Higgs bosons at the LHC for m_A up to several hundred GeV [24]. We will come back to the importance of determining m_A later in Sec. 3.

In Fig. 1 and 2, we only looked into the parameter space with moderate (“natural”) values of m and M . If $m \gg M$, solutions with $\mu \sim M$ may be obtained [19, 25], and the assumption $\tilde{\chi}_1^0 \simeq \tilde{B}$ is not valid any more. In such a case the decay $\tilde{\chi}_2^0 \rightarrow \tilde{e}_R$ is not open. However there is still a chance that wino-like charginos and neutralinos ($\tilde{\chi}_4^0$ and $\tilde{\chi}_2^+$) are produced in cascade decays, and yield additional kinematic constraints besides the end point measurement of the m_{ll} distribution from $\tilde{\chi}_2^0 \rightarrow \tilde{\chi}_1^0 ll$ decay; see Sec. 3. Large m may also be allowed when $m_{\tilde{\chi}_1^0} \sim m_Z/2$, in which case $\tilde{\chi}_2^0 \rightarrow \tilde{e}_R$ need not be open to make $\Omega_{\tilde{\chi}_1^0}$ small. Even then the m_{ll} end point determines $m_{\tilde{\chi}_2^0} - m_{\tilde{\chi}_1^0}$ [5, 26], and the m_{ll} distribution of three body $\tilde{\chi}_2^0$ decays is sensitive to very large $m_{\tilde{e}_R}$ [27]. Another twist appears when $\tilde{\chi}_2^0 \rightarrow \tilde{\chi}_1^0 Z$ is open and dominates $\tilde{\chi}_2^0$ decays. The small leptonic branching ratio of the Z boson might then make it difficult to study neutralino masses, and there is no sensitivity to slepton masses. Note, however, that in the bino-dominant region $\tilde{\chi}_2^0 \rightarrow Z$ decays cannot compete with $\tilde{\chi}_2^0 \rightarrow \tilde{e}_R$ decays unless the latter are strongly phase space suppressed.

We already briefly alluded to the case where $m_{\tilde{e}_R} \gg m_{\tilde{\tau}_1}$ due to renormalization group effects and $\tilde{\tau}$ mixing. The lighter $\tilde{\tau}$ can be substantially lighter than the other sleptons if $\mu \tan \beta$ is large [22]. In this case pair annihilation through t channel $\tilde{\tau}$ exchange can even dominate other sparticle exchange contributions [19], because $\tilde{\tau}_1$ could be lighter than the

other sparticles, and the mixing induces an S -wave amplitude. In [28] the possibility to detect and study $\tilde{\tau}$ at the LHC is discussed. The end point of the $j_\tau j_\tau$ invariant mass distribution, where j_τ denotes a τ -jet, is not as well determined as that of the m_{ll} distribution, but it has been estimated that a $\sim 5\%$ measurement should be possible. Even if the $j_\tau j_\tau$ end point indicates $m_{\tilde{\tau}_1} < m_{\tilde{e}_R}$, the constraint on $m_{\tilde{q}}$, $m_{\tilde{\chi}_2^0}$ and $m_{\tilde{\chi}_1^0}$ from ll events originating from $\tilde{\chi}_2^0 \rightarrow \tilde{e}_R$ decays can perhaps be used to reduce the $m_{\tilde{\tau}}$ error, in which case the combined error should not increase too much. However, if $\tan\beta$ is very large, it becomes easier to have an acceptable LSP relic density even if $m_{\tilde{e}_R} > m_{\tilde{\chi}_2^0}$. In this case one may need a linear collider to perform precision measurements of the nature of $\tilde{\tau}_1$ [29, 30], where $\sigma_{\tilde{\tau}_1}$, the end point of the τ jet energy distribution, and a measurement of the τ polarization would do a good job in determining the parameters needed to predict the thermal LSP relic density.

3 $\Omega_{\tilde{\chi}_1^0}$ in non-mSUGRA scenarios and collider signals

In the previous section, we have shown that the mSUGRA assumption predicts a bino-dominant LSP. We also found that measurements at LHC experiments are sufficient for a prediction of $\Omega_{\tilde{\chi}_1^0} h^2$, if the cascade decay $\tilde{\chi}_2^0 \rightarrow \tilde{e}_R \rightarrow \tilde{\chi}_1^0$ is open and LSP bino dominance is assumed. Now the question is if LHC experiments can be used to check the assumption that the LSP is mostly a bino. After all, it is possible that μ is smaller than or of the order of the gaugino masses, and that the mSUGRA relation $M_1 \simeq M_2/2$ is broken. In this and the following Section, we discuss a scenario where the inequality $M_1 < M_2$ is kept, while μ is substantially smaller than the mSUGRA prediction. In such a case Z exchange effects and/or LSP annihilation into W pairs are expected to be more important than in the strict mSUGRA scenario studied in the previous Section, and one needs more information to predict the thermal contribution to $\Omega_{\tilde{\chi}_1^0} h^2$.

The relative size between μ and M is controlled by Higgs sector mass parameters. The MSSM Higgs potential can be written as

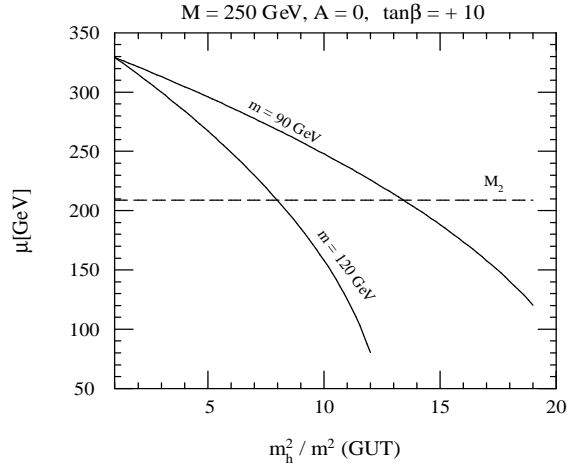
$$V = (m_1^2 + \mu^2)H_1^\dagger H_1 + (m_2^2 + \mu^2)H_2^\dagger H_2 + (B\mu H_1 \cdot H_2 + h.c.) + (4\text{th order terms}). \quad (6)$$

Here m_1 and m_2 are soft breaking Higgs masses. In the previous Section we took $m_1 = m_2 = m$ at the GUT scale, which gave $\mu^2 \gg M^2$ unless $m^2 \gg M^2$. In general, $|\mu| \sim M$ may be achieved by allowing non-universal soft breaking Higgs masses, $m_1, m_2 \neq m$. For simplicity we will keep $m_1 = m_2 \equiv m_h$ at the GUT scale; we briefly comment on the effect of relaxing this assumption below.

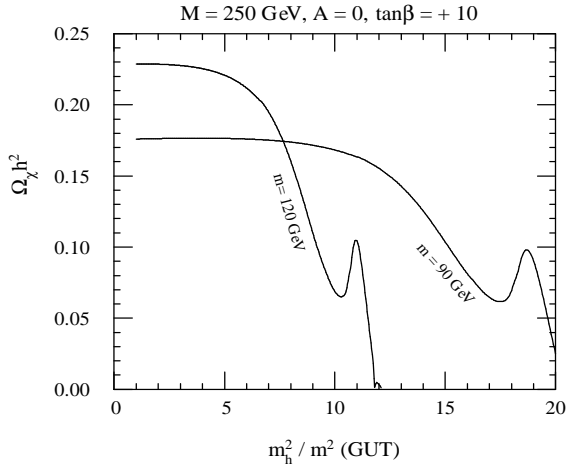
In Fig 3a), we plot $|\mu|$ vs. $(m_h/m)^2$. By increasing m_h , μ is reduced gradually so that $m_h^2 + \mu^2$ at the GUT scale is roughly constant. Note that the negative radiative correction to Higgs mass m_2^2 is dominated by the gaugino mass through the stop and sbottom masses for this choice of parameters³. Therefore the value of m_h^2 giving $|\mu| \sim M_2$ is almost independent of m , $m_h \sim 330$ GeV. Generally $|\mu| \sim M$ can be achieved if $m_h|_{GUT} \gtrsim M$; the precise value is determined by the top Yukawa coupling. In Fig. 3b) and 3c), we also plot $\Omega_{\tilde{\chi}_1^0}$ and the b factor. These quantities vary substantially once $|\mu|$ falls below M_2 .

In Fig. 4 we show contours of constant $\Omega_{\tilde{\chi}_1^0}$ and constant b factor in the $(m_h^2/m^2, M)$ plane for fixed $m = 100$ GeV. We first note that $\Omega_{\tilde{\chi}_1^0}$ decreases as m_h is increased. This is due to the reduction of $|\mu|$ for larger m_h , see Fig. 3. This increases the higgsino components of $\tilde{\chi}_1^0$ and

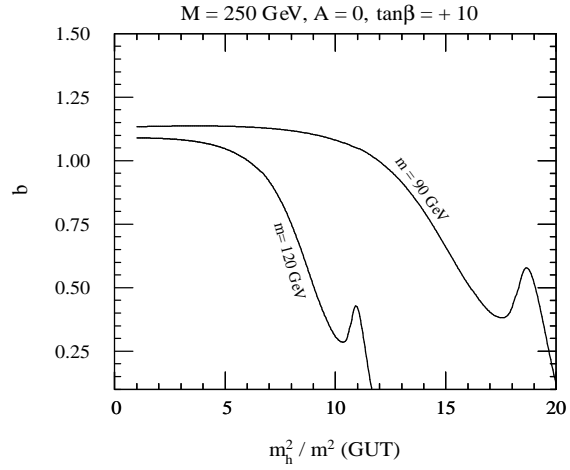
³The fact that in mSUGRA m_2^2 at the weak scale is almost independent of m^2 is closely related to the “focus point” behavior studied in ref.[25].



a)



b)



c)

Figure 3: a) μ b) $\Omega_{\chi_1^0}$ and c) b as function of $(m_h/m)^2$. We fix $M = 250 \text{ GeV}$, $A = 0$ and $\tan\beta = 10$.

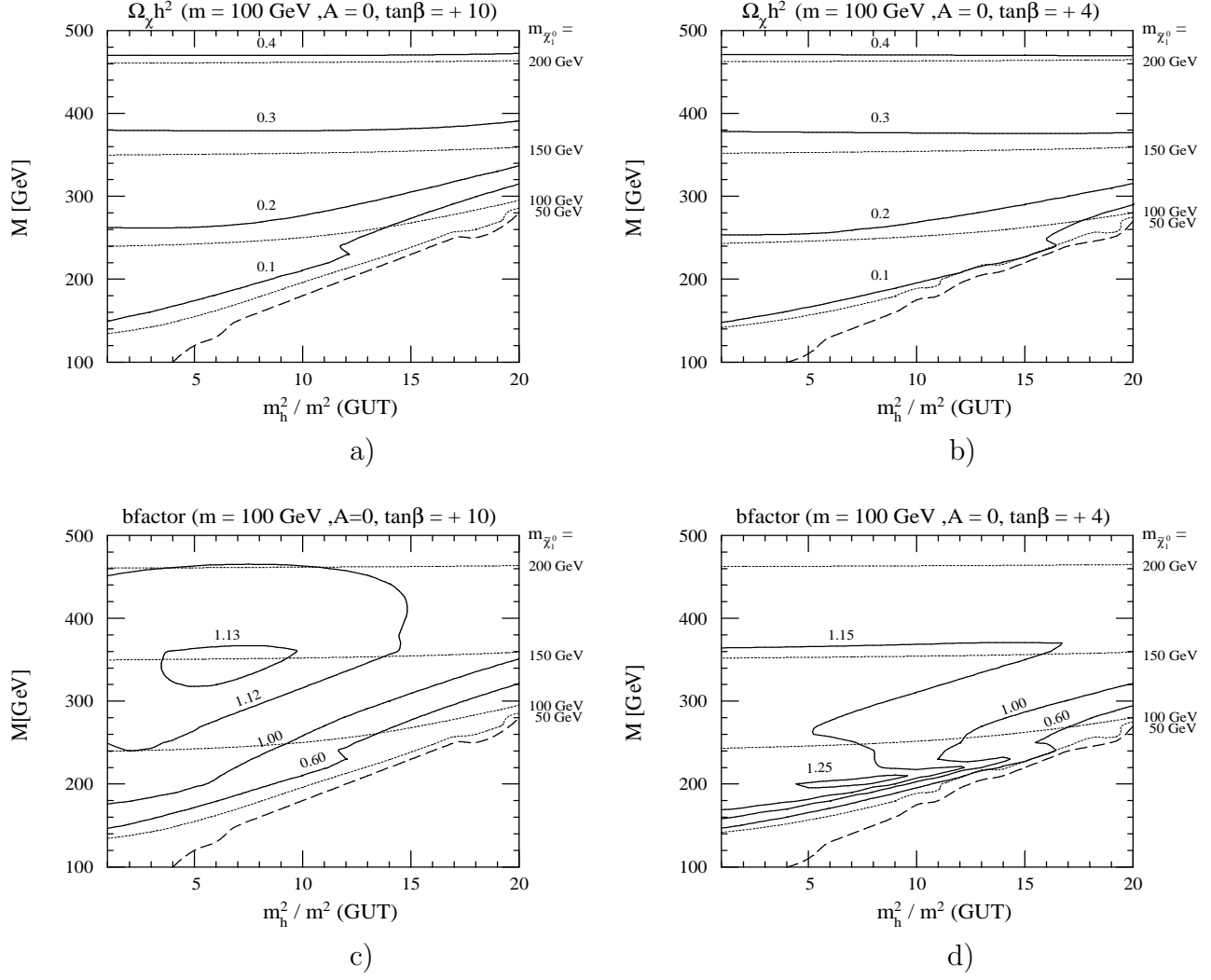


Figure 4: $\Omega_{\tilde{\chi}_1^0}$ and the b factor in the $(m_h^2/m^2, M)$ plane for fixed m .

also reduces its mass. Not only $\Omega_{\tilde{\chi}_1^0}$ but also the b factor decreases, therefore pair annihilation is no longer dominated by sfermion exchanges. Especially in Fig. 4d) we find very strong effects from LSP annihilation into W pairs. The same effect also can be found in Fig. 3b and c), where the rise of b and $\Omega_{\tilde{\chi}_1^0}$ corresponds to the closure of the WW mode. Note that no consistent solution with electroweak symmetry breaking exists below and to the right of the dashed line.⁴

As mentioned earlier we assume the two soft breaking Higgs masses to be the same at the GUT scale. However, once $\tan^2 \beta \gg 1$, the higgsino mass $|\mu|$ is essentially only sensitive to the value of m_2^2 . One can therefore increase or reduce the pseudoscalar Higgs mass by varying m_1^2 at the GUT scale without affecting μ at the weak scale significantly. Nevertheless, as long as $m_1^2(M_X) > 0$ and $\tan \beta$ is not very large, $m_A = \sqrt{m_1^2 + m_2^2 + 2\mu^2}|_{\text{weak}}$ remains well above $2m_{\tilde{\chi}_1^0}$. However, in principle there is nothing wrong with having $m_1^2(M_X) < 0$, as long as the “boundedness condition” $m_1^2 + m_2^2 > 2|B\mu|$ remains satisfied at all scales. If $m_A \simeq 2m_{\tilde{\chi}_1^0}$, the thermal LSP relic density is very small. Strictly speaking the constraints on $\Omega_{\tilde{\chi}_1^0} h^2$ that we will derive below are therefore merely upper bounds as long as we cannot prove experimentally that m_A is well above $2m_{\tilde{\chi}_1^0}$.

The reduction of $|\mu|$ would alter SUSY signals at colliders significantly. When $|\mu| \lesssim M$, $\tilde{\chi}_4^0$ and $\tilde{\chi}_2^+$ production from the decay of $SU(2)$ doublet squarks becomes important as they have substantial wino component. This leaves an imprint on the kinematics of di-lepton events, which gives us access to additional MSSM parameters, especially when the decay channels of neutralinos and charginos into real sleptons are open. This increases the statistics of clean ll +jets+missing P_T events, since the channels

$$\begin{aligned} \tilde{\chi}_2^+ &\rightarrow \tilde{\nu}_L^{(*)} \rightarrow \tilde{\chi}_1^+ \\ \tilde{\chi}_4^0 &\rightarrow \tilde{e}_L^{(*)}(\tilde{e}_R^{(*)}) \rightarrow \tilde{\chi}_2^0(\tilde{\chi}_1^0) \end{aligned} \quad (7)$$

should be seen in addition to the conventional $\tilde{\chi}_2^0 \rightarrow \tilde{\chi}_1^0 ll$ signal.⁵

As a result,

1. The m_{ll} edge, and the other end points of the jl and jll invariant mass distributions of $\tilde{\chi}_2^+ \rightarrow \tilde{\nu}_L \rightarrow \tilde{\chi}_1^+$ may be measured. By identifying τ -leptons from $\tilde{\chi}_1^+$ decay, one can confirm experimentally that the cascade decay originates from $\tilde{\chi}_2^+$. This gives lower *and* upper bounds on $|\mu|$, which in turn constrain the size of the higgsino component of the LSP. An explicit example will be analyzed in Sec. 4.
2. $\tilde{\chi}_4^0$ may decay into \tilde{e}_L directly followed by \tilde{e}_L decay into $\tilde{\chi}_2^0$ or $\tilde{\chi}_1^0$. On the other hand the decay $\tilde{\chi}_2^0 \rightarrow \tilde{e}_L$ is usually forbidden or kinematically suppressed. Therefore $\tilde{\chi}_2^0$ decays and $\tilde{\chi}_4^0$ decays give information on different slepton masses.

Note that there are substantial constraints on -ino masses and slepton masses from $SU(2) \times U(1)$ gauge invariance. The six chargino and neutralino masses are determined (up to radiative

⁴Right on this line electroweak symmetry breaking requires $\mu = 0$. Searches for neutralino and chargino production at LEP therefore exclude the region just above the dashed line. However, this experimentally excluded region is very narrow, since $|\mu|$ varies very rapidly near the maximal allowed value of m_h , as shown in Fig. 3.

⁵ When M_1 and M_2 have the same sign and $|\mu|$ is not too small, one of the neutralinos is very higgsino-like and would not be produced from the first and second generation squark decays. Here we implicitly assume $M_1 < \mu \lesssim M_2$, in which case the higgsino-like state is $\tilde{\chi}_3^0$.

corrections [31]) by the values of the four parameters M_1 , M_2 , μ and $\tan\beta$, while $m_{\tilde{e}_L}$ and $m_{\tilde{\nu}}$ are related by

$$m_{\tilde{\nu}}^2 - m_{\tilde{e}_L}^2 = m_Z^2 \cos^2 \theta_W \cos 2\beta \quad (8)$$

Therefore the measured edges and end points originating from several decay chains can over-constrain the relevant MSSM parameters.

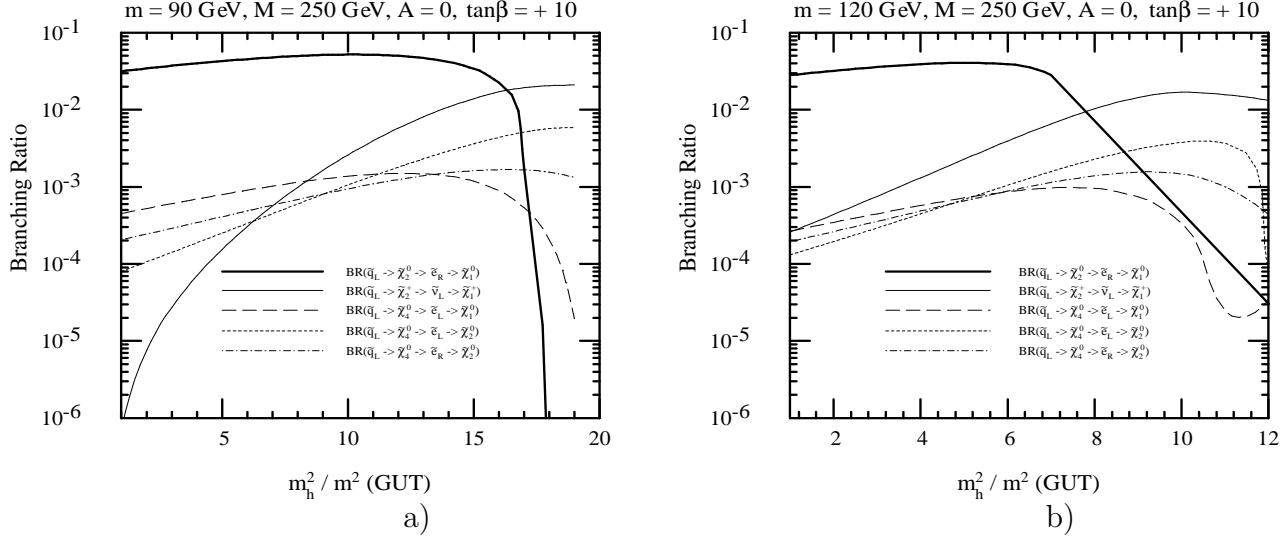


Figure 5: Squark decay branching ratios for a) $m = 90$ GeV and b) $m = 120$ GeV, for $M = 250$ GeV, $A = 0$ and $\tan\beta = 10$. We average \tilde{u}_L and \tilde{d}_L decay branching ratios.

In Fig. 5, we show various \tilde{q}_L decay branching ratios, defined as an average of \tilde{u}_L and \tilde{d}_L branching ratios. As m_h increases we find substantial branching ratios into the heavier neutralino and chargino, once $|\mu|$ becomes comparable to M_2 . The sources of the rise of the of $\tilde{\chi}_2^+$ signal are:

1. The increase of squark branching ratios into $\tilde{\chi}_2^+$ and $\tilde{\chi}_4^0$ with increasing wino component. In the limit $|\mu| \ll M_2$ the branching ratios satisfy (assuming $M_1 < M_2$):

$$Br(\tilde{q}_L \rightarrow \tilde{\chi}_2^+) : Br(\tilde{q}_L \rightarrow \tilde{\chi}_4^0) : Br(\tilde{q}_L \rightarrow \tilde{\chi}_1^+) = 2 : 1 : 0. \quad (9)$$

Throughout Fig. 5, $\tilde{\chi}_3^0$ is a nearly pure higgsino and does not have a substantial branching ratio. See Table 2 in Sec. 4 for an explicit example.

2. The growth of the $\tilde{\chi}_2^+$ decay branching ratio into $\tilde{\nu}_L l$, again due to the increase of its wino component. Note that $\tilde{\chi}_2^+ \rightarrow \tilde{\nu}_L$ is kinematically favored compared to $\tilde{\chi}_2^+ \rightarrow \tilde{e}_L$.
3. There is little or no phase space for $\tilde{\nu}_L$ decays into $\tilde{\chi}_1^+ l$ if $M_2 < |\mu|$. On the other hand, this mode may open up when $\tilde{\chi}_1^+$ becomes higgsino-like. Indeed for Fig. 5a), in the region of small m_h the decay $\tilde{\nu}_L \rightarrow \tilde{\chi}_1^+$ is suppressed due to the near mass degeneracy between $\tilde{\nu}_L$ and $\tilde{\chi}_1^+$.
4. Finally, “conventional” modes such as $\tilde{q} \rightarrow \tilde{\chi}_1^+$ and $\tilde{q} \rightarrow \tilde{\chi}_2^0$ will be suppressed due to the reduced gaugino components of these light states. Moreover, the decay $\tilde{\chi}_2^0 \rightarrow \tilde{e}_R$ may be suppressed or closed kinematically even for small values of m , if $|\mu| < M_2$. In the limit $|\mu| < M_1$, $m_{\tilde{\chi}_2^0} - m_{\tilde{\chi}_1^0}$ is small, and the corresponding m_{ll} distribution might be too soft to be accessible experimentally.

These observations tell us that one should look for $\tilde{\chi}_2^+$ and $\tilde{\chi}_4^0$ signals in addition to conventional $\tilde{\chi}_2^0 \rightarrow \tilde{\chi}_1^0 l^+ l^-$ decays. Discriminating experimentally between scenarios with $|\mu| > M$, where these new signals are small, and $|\mu| < M_2$, where they are expected to be significant, would be important to predict the mass density of the Universe. In the next Section we illustrate how these new signals could be analyzed at the LHC.

4 Analyzing the MSSM with $|\mu| \sim M$ at the LHC

4.1 A Monte Carlo Study

m	90.0	$\tan \beta$	10	m_1	360	m_2	360
M	250	μ	199.85	M_1	103.9	M_2	208.75
$m_{\tilde{e}_R}$	139.3	$m_{\tilde{e}_L}$	206.09	$m_{\tilde{u}_L}$	556.07	$m_{\tilde{d}_L}$	561.67
$m_{\tilde{\nu}}$	190.28	$m_{\tilde{\chi}_1^0}$	93.18	$m_{\tilde{u}_R}$	534.36	$m_{\tilde{d}_R}$	533.21
$m_{\tilde{\chi}_2^0}$	155.13	$m_{\tilde{\chi}_3^0}$	208.74	$m_{\tilde{\chi}_1^+}$	148.44	$m_{\tilde{\chi}_2^+}$	272.52
$m_{\tilde{\chi}_4^0}$	273.8	$m_{\tilde{\nu}_\tau}$	188.67	$m_{\tilde{t}_1}$	374.43	$m_{\tilde{t}_2}$	563.81
$m_{\tilde{\tau}_1}$	132.56	$m_{\tilde{\tau}_2}$	206.06	$m_{\tilde{b}_1}$	498.27	$m_{\tilde{b}_2}$	531.2
m_h	112.59	m_P	436.98	m_H	437.63	$m_{\tilde{g}}$	624.36

Table 1: Mass parameters and relevant sparticle masses in GeV for the point studied in this paper. ISAJET [32] was used to generate this spectrum.

We now study leptonic SUSY signals at the LHC for a case where $\tilde{\chi}_2^+$ production from \tilde{q}_L decays is sufficiently common to be detectable. We used ISAJET 7.42 [32] to generate signal events, while ATLFast 2.21 [33] was used to simulate the detector response. For this analysis we choose the MSSM parameter point shown in Table 1. Here we took a moderate value for M , leading to a large sample of signal events.

The value of the GUT scale Higgs mass is chosen such that the \tilde{B} component of $\tilde{\chi}_1^0$ $N_{\tilde{B}} = 0.9$, so that effects from its other components on the predicted LSP relic density start to be significant; $(N_{\tilde{B}}, N_{\tilde{W}}, N_{\tilde{H}_1}, N_{\tilde{H}_2}) = (0.91, -0.15, 0.19, -0.35)$. In ISAJET this requires $m_h/m = 4$. Our one-loop RG analysis described in Sec. 3 reproduces this point for $m_h/m \sim 3.74$, see Fig. 3a. See also Figs. 3b) and 3c) for the corresponding values of $\Omega_{\tilde{\chi}_1^0}$ and the b factor. Reducing $|\mu|$ even further (by increasing m_h) would lead to even larger differences to well-known mSUGRA scenarios, making it easier to measure all relevant parameters.

In pp collisions one mostly produces squarks and gluinos. They decay further into neutralinos and charginos. In our case gluinos do not decay exclusively into third generation squarks; the branching ratio into first and second generation left handed squarks is about 20% (11.3% into \tilde{u}_L and 9.6% into \tilde{d}_L). These squarks then often decay into $\tilde{\chi}_2^+$ and $\tilde{\chi}_4^0$. The branching ratios relevant for the following discussions are summarized in Table 2. The tiny branching ratio into $\tilde{\chi}_3^0$ is due to the fact that it is mostly higgsino. In Table 3 we show the dominant cascade decay processes which produce opposite sign same flavor lepton pairs in the final state. In this Table we also list the corresponding end points of the kinematic distributions discussed in Sec. 2, see eqs.(3) and (4).

We now show several SUSY event distributions, after applying the following cuts [26] to reduce the SM background to a negligible level:

$\tilde{u}_L \rightarrow \tilde{\chi}_2^0$	20.7	$\tilde{d}_L \rightarrow \tilde{\chi}_2^0$	14.5
$\tilde{u}_L \rightarrow \tilde{\chi}_3^0$	0.4	$\tilde{d}_L \rightarrow \tilde{\chi}_3^0$	0.7
$\tilde{u}_L \rightarrow \tilde{\chi}_4^0$	12.2	$\tilde{d}_L \rightarrow \tilde{\chi}_4^0$	15.4
$\tilde{u}_L \rightarrow \tilde{\chi}_2^+$	21.4	$\tilde{d}_L \rightarrow \tilde{\chi}_2^+$	36.4
$\tilde{\chi}_2^0 \rightarrow \tilde{e}_R$	23.6	$\tilde{\chi}_4^0 \rightarrow \tilde{e}_L$	5.5
$\tilde{\chi}_2^+ \rightarrow \tilde{\nu}_L$	9.7	$\tilde{\chi}_4^0 \rightarrow \tilde{e}_R$	1.1
$\tilde{\chi}_1^+ \rightarrow \tilde{\tau}_1$	89.1	$\tilde{\nu}_L \rightarrow \tilde{\chi}_1^+$	40.1
$\tilde{e}_L \rightarrow \tilde{\chi}_2^0$	38.2	$\tilde{e}_R \rightarrow \tilde{\chi}_1^0$	100
$\tilde{e}_L \rightarrow \tilde{\chi}_1^0$	19.8		

Table 2: Relevant branching ratios in % for our sample parameters.

mode	m_{jl}^{\max}	m_{jl}^{\min}	m_{jll}^{\max}	m_{jll}^{\min}	m_{ll}^{\max}
D1) $\tilde{q}_L \rightarrow \tilde{\chi}_2^0 \rightarrow \tilde{e}_R \rightarrow \tilde{\chi}_1^0$	400.3	237.0	430.6	164.2	50.6
D2) $\tilde{q}_L \rightarrow \tilde{\chi}_2^+ \rightarrow \tilde{\nu}_L \rightarrow \tilde{\chi}_1^+$	351.0	260.0	411.1	211.1	121.9
D3) $\tilde{q}_L \rightarrow \tilde{\chi}_4^0 \rightarrow \tilde{e}_L \rightarrow \tilde{\chi}_2^0$	322.7	269.5	403.3	207.5	117.9
D4) $\tilde{q}_L \rightarrow \tilde{\chi}_4^0 \rightarrow \tilde{e}_L \rightarrow \tilde{\chi}_1^0$	437.0	321.4	460.6	246.6	159.6
D5) $\tilde{q}_L \rightarrow \tilde{\chi}_4^0 \rightarrow \tilde{e}_R \rightarrow \tilde{\chi}_1^0$	421.5	292.2	460.6	270.3	174.3

Table 3: End points or edges of invariant mass distributions (in GeV) for different decay processes.

- 4 jets with $P_{T,1} > 100$ GeV and $P_{T,2,3,4} > 50$ GeV.
- $M_{\text{eff}} \equiv P_{T,1} + P_{T,2} + P_{T,3} + P_{T,4} + \cancel{E}_T > 400$ GeV.
- $\cancel{E}_T > \text{Max}(100 \text{ GeV}, 0.2 M_{\text{eff}})$.
- Two isolated leptons with $P_T^l > 10$ GeV and $|\eta| < 2.5$. Isolation is defined as having less than 10 GeV energy deposited in a cone with $\Delta R = 0.2$ around the lepton direction.

In the following plots we reduce SUSY backgrounds by subtracting event samples with different flavor, opposite sign dileptons ($e^+\mu^-$ and μ^-e^+) from the sum of the e^+e^- and $\mu^+\mu^-$ event samples. To do this consistently we require two and only two isolated leptons in the final state.⁶ We generated events corresponding to an integrated luminosity of 200 fb^{-1} , but the figures are normalized to 100 fb^{-1} .

In Fig. 6 we show the di-lepton invariant mass distribution for our representative point. After the subtraction of $e\mu$ events, we see a distribution with at least four edges.⁷ They are consistent with those found in Table 3. Note that a rather weak edge from decay D3) should appear very close to the one from D2) in both the $M \gg |\mu|$ and $|\mu| \gg M$ limit; $m_{\tilde{\chi}_2^+} \sim m_{\tilde{\chi}_4^0}$,

⁶However, as we have discussed in previous Sections, the rates of 4 and 3 lepton events compared to 2 lepton events must contain important information about MSSM parameters.

⁷Note that at $m_{ll} \sim 55$ GeV, this subtraction reduces the number of events by a factor of 0.35. The fluctuation of the resulting distribution is therefore higher than what is expected from the number of events in this distribution.

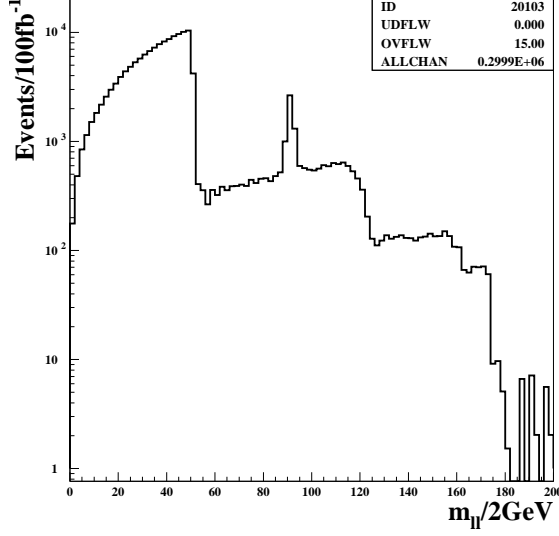


Figure 6: The $m_{e^+e^-} + m_{\mu^+\mu^-} - m_{e^+\mu^-} - m_{e^-\mu^+}$ distribution for the parameter point listed in Table 1.

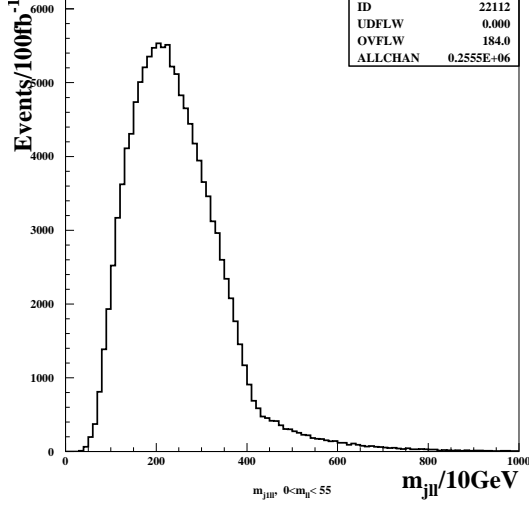
$m_{\tilde{\chi}_2^0} \sim m_{\tilde{\chi}_1^+}$ and $m_{\tilde{\nu}} \sim m_{\tilde{e}_L}$ hold in a wide region of parameter space. The two edges must be separated out by fitting the smeared m_{ll} distribution. Note that since the kinematics of two decay chains is expected to be similar, the systematic errors associated with the fitting should be small. It seems that at least the first four m_{ll} edges can be used for the fit of MSSM parameters, while it is not clear if the last one is detectable statistically.

We then follow the analysis of [14], by taking the jets with the first and the second largest P_T and considering their m_{jll} distributions. We label j_1 and j_2 so that $m_{j_1ll} < m_{j_2ll}$. We then find that most events have m_{j_1ll} below ~ 400 GeV. The m_{jll} distribution will contain events from the different decay chains listed in Table 3, but they can easily be separated out by requiring m_{ll} to lie between certain values. For example, if we require that $m_{ll} < 55$ GeV (Fig. 7a) and $55 < m_{ll} < 125$ GeV (Fig. 7b), the distributions should dominantly contain events from decay chains D1) and D2), respectively. In Fig. 7a) the m_{jll} end points are indeed consistent with the values of end points listed in Table 3. The distribution in Fig. 7b) is somewhat smeared out near the end point, due to contamination from $\tilde{\chi}_4^0$ decays.

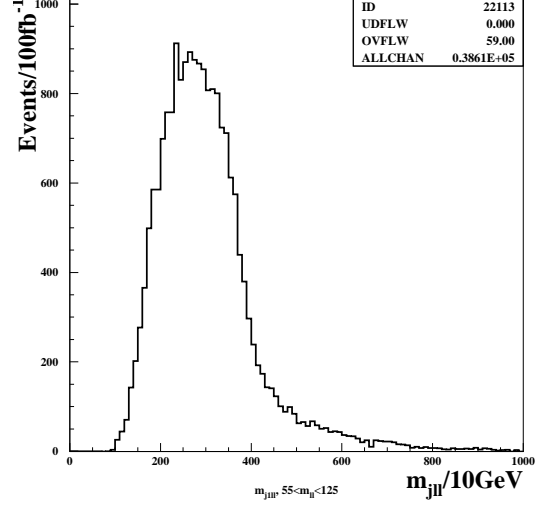
In the next step we select events where $m_{j_1ll} < 500$ GeV $< m_{j_2ll}$; the resulting m_{jll} distributions are shown in Figs. 7c) and 7d). These additional cuts have been applied in ref.[14] because they reduce the probability to select the “wrong” jet, which does not come from primary \tilde{q}_L decays. The m_{j_1ll} distribution is then substantially harder, better reflecting the distribution of the “correct” jet. Especially for events with 55 GeV $< m_{ll} < 125$ GeV, the m_{j_1ll} end point of decay D2) can be seen more clearly over the distributions from $\tilde{\chi}_4^0$ decays D4) and D5), which have higher m_{j_1ll} edges.

In Figs. 7c) and d), we nevertheless see some continuous background near the end point of m_{j_1ll} which cannot be explained by $\tilde{\chi}_4^0$ contamination. Note that for our choice of parameters, \tilde{q}_L is considerably lighter than for the case studied in [14]; moreover, $m_{\tilde{\chi}_2^+}$ is not too small compared to $m_{\tilde{q}}$. The probability that one of the two hardest jets does not come from primary squark decays should therefore be higher than in the example analyzed in ref.[14].

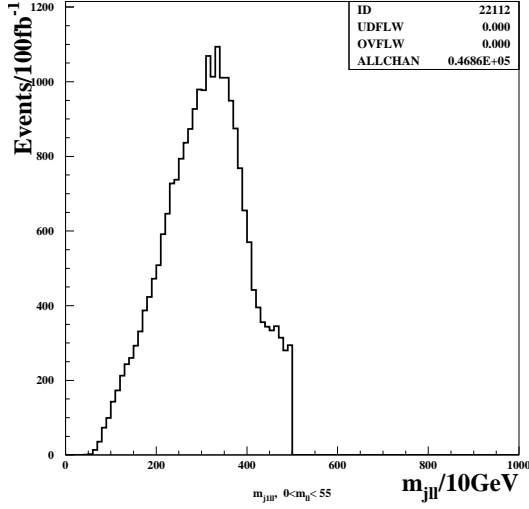
These mis-reconstructed events also contaminate the $m_{j_1ll}^{\max}$ edge if we demand $m_{j_1ll} < 500$ GeV $< m_{j_2ll}$, as can be seen in Figs. 8a), b). Here we plot the higher of the two m_{j_1l}



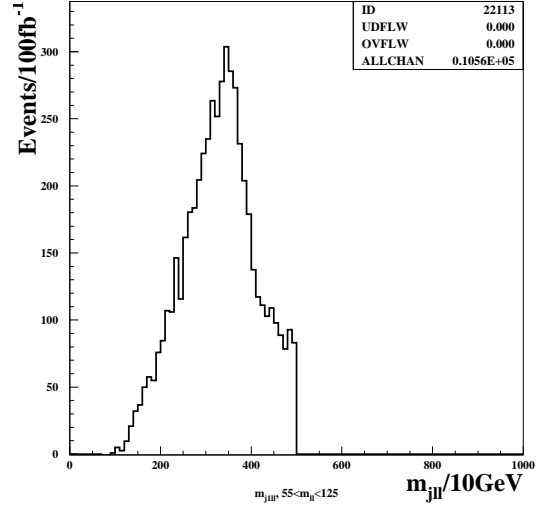
a)



b)

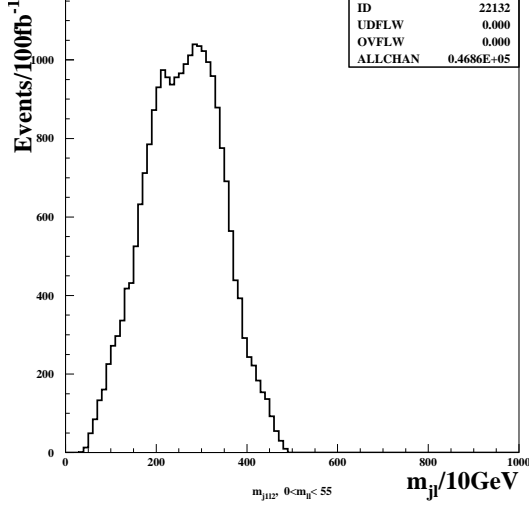


c)

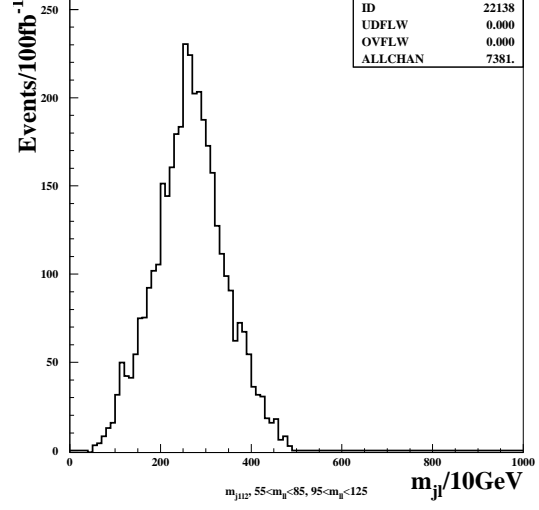


d)

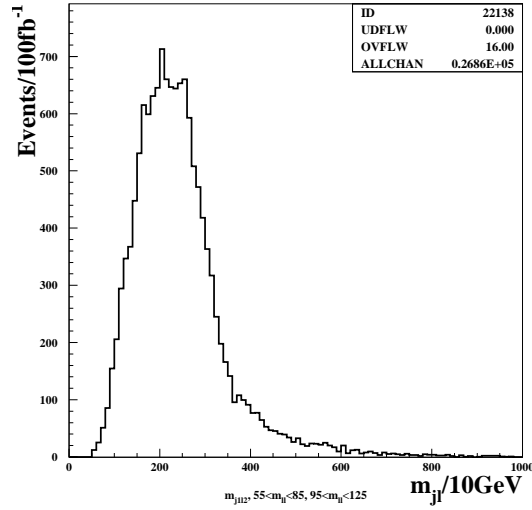
Figure 7: a), b): m_{j1l} distributions for a) $m_{ll} < 55$ GeV, b) $55 \text{ GeV} < m_{ll} < 125$ GeV. c), d): The same distributions after requiring $m_{j1l} < 500 \text{ GeV} < m_{j2l}$.



a)



b)



c)

Figure 8: Distribution of the higher of the two $m_{j_1 l}$ values for a) $0 < m_{ll} < 55$ GeV, b) $55 \text{ GeV} < m_{ll} < 85$ GeV or $95 \text{ GeV} < m_{j_1 l} < 125$ GeV with the cuts $m_{j_1 l} < 500 \text{ GeV} < m_{j_2 l}$. Figure c) corresponds to b) without the cuts on $m_{j_1 l}$ and $m_{j_2 l}$.

values in each event. However, the edges seem to be higher than the expected values in Table 3. Note that we exclude events with $m_{ll} \sim m_Z$ because $\tilde{\chi}_2^+ \rightarrow Z\tilde{\chi}_1^+$ followed by $Z \rightarrow ll$ has a higher m_{jll} edge. For the sample with $m_{ll} < 55$ GeV, the contamination is seen as a change of slope, while for the samples with $55 \text{ GeV} < m_{ll} < 85$ GeV or $95 \text{ GeV} < m_{ll} < 125$ GeV, no structure can be seen near the expected end point.

This contamination actually was to be expected, because the events that fall above the real m_{jll} edge must be mis-reconstructed events where the jet originates from another sparticle decay or QCD radiation. Therefore the corresponding m_{jl} has no need to respect m_{jl}^{\max} , either; it tends to have a value larger than this nominal end point. The artificial upper limit of the m_{jll} distribution imposed by the cut then distorts the event distribution in Fig. 8 b). We find that the m_{jll} distribution *without* the requirement $m_{jll} < 500 \text{ GeV} < m_{j2ll}$ reproduces the m_{jl}^{\max} end point of decay chain D2) better for the events with $125 \text{ GeV} > m_{ll} > 95$ or $85 \text{ GeV} > m_{ll} > 55$ GeV (Fig. 8c), although the distribution is still affected somewhat by events coming from $\tilde{\chi}_4^0$ decays.

The lower edge m_{jll}^{\min} may be reconstructed from the m_{j2ll} distribution requiring $m_{ll} \geq m_{ll}^{\max}/\sqrt{2}$; see Fig. 9. This distribution is much harder than the corresponding $e\mu$ distribution; this is a sign that the observed lower edge is real. The fit of the end point distributions will be given elsewhere [34].

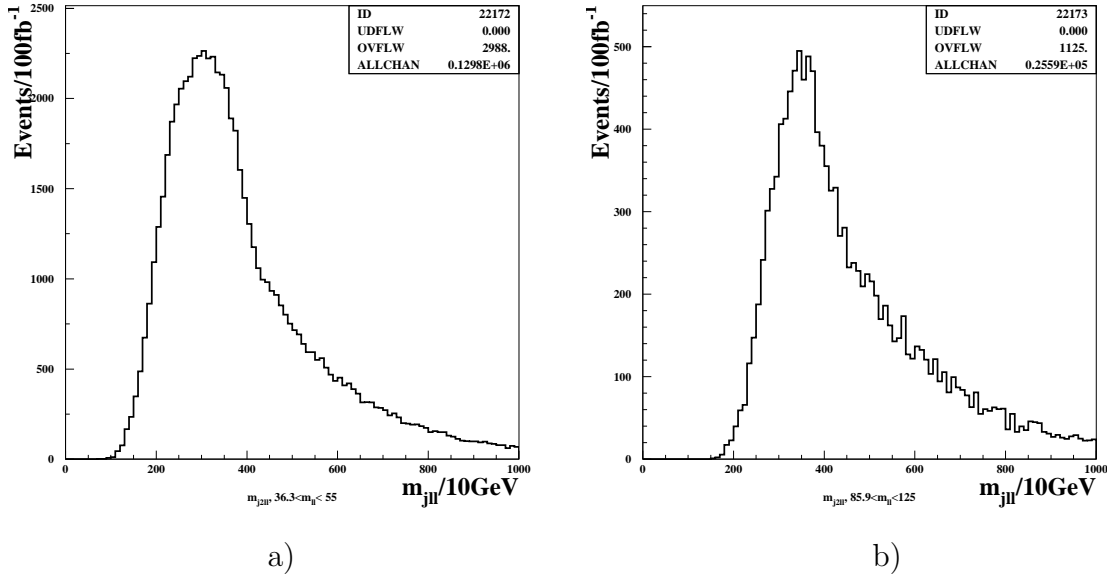


Figure 9: m_{j2ll} distribution for a) $36.3 \text{ GeV} < m_{ll} < 55 \text{ GeV}$ and b) $85.9 \text{ GeV} < m_{ll} < 125 \text{ GeV}$.

We now discuss the possibility to identify $\tilde{\chi}_2^+$ decays through the chain D2). In this case most daughter $\tilde{\chi}_1^+$'s would decay further as $\tilde{\chi}_1^+ \rightarrow \tilde{\tau}_1 \rightarrow \tilde{\chi}_1^0$, see Table 2, producing a τ lepton in the last step of the cascade decay. The τll invariant mass never exceeds $m_{\tilde{\chi}_2^+} - m_{\tilde{\chi}_1^0}$. Hadronic τ decays might be identified by looking for a narrow jet that is isolated from other jet activity. Instead of studying the jet selection, we use information from the event generator to choose jets consistent with the parent τ direction in the event list. The jet with minimum dR is selected as τ -jet if $dR < 0.3$, $|\eta| < 2.5$ and $P_T/P_{Tj} > 0.9$, where $P = P_\tau - P_{\nu_\tau}$. We plot the $m_{j\tau ll}^{\min}$ distribution, where j_τ is selected so that $m_{j\tau ll}$ is minimal if the event contains several τ -jets. When we compare the distributions for $m_{ll} < 55$ GeV (Fig. 10a) and $55 \text{ GeV} < m_{ll} < 125$ GeV (Fig. 10b), we find the latter events clustered in the region $m_{j\tau ll} < 190$ GeV, while no

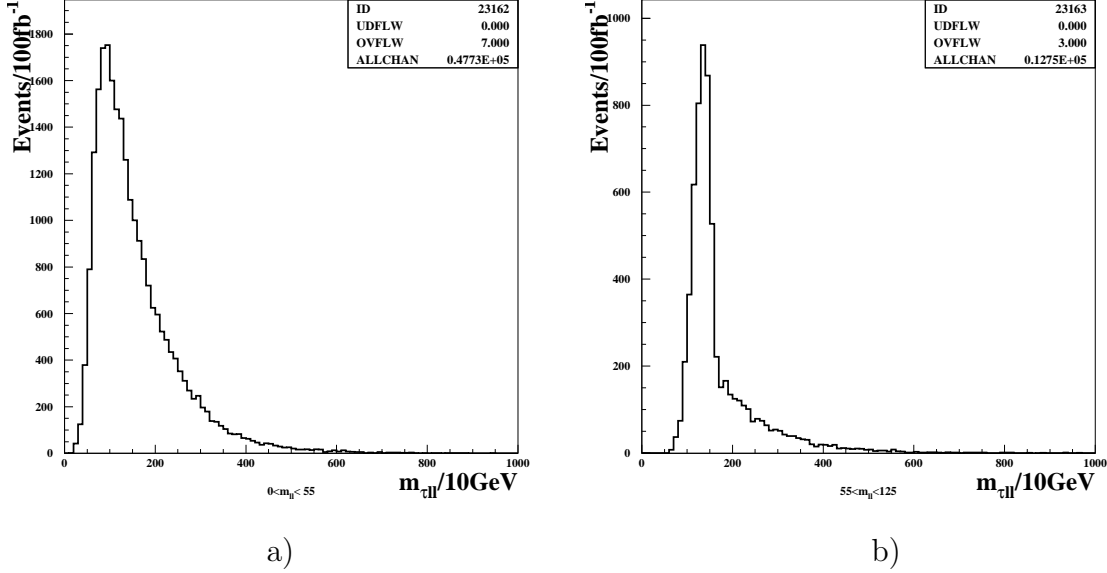


Figure 10: The invariant mass distribution $m_{j\tau ll}$ for a) $m_{ll} < 55$ GeV and b) for $55 \text{ GeV} < m_{ll} < 125$ GeV.

such structure is found for the events with $m_{ll} < 55$ GeV. The only possible interpretation would be that most ll pairs with $55 \text{ GeV} < m_{ll} < 125$ GeV stem from the decay of a charged particle, $\tilde{\chi}_2^+$.

In the above plot, we are assuming 100% acceptance of τ jets and no contamination from QCD jets. A rejection factor of $O(10^2)$ against QCD jets together with a 40% τ identification efficiency might be possible in the ATLAS experiment for jets with $P_T > 30$ GeV [24]. In [28], the fake tau distribution is studied assuming a rejection factor of 15 for the case where $\tilde{\chi}_2^0$ decays dominantly into $\tau^+\tau^-\tilde{\chi}_1^0$. Fake τ backgrounds are then sizable in the region above the edge of the signal $\tau^+\tau^-$ distribution. The use of the $j_\tau ll$ distribution to clean up the $\tilde{\chi}_2^+$ sample might nevertheless help to reconstruct edges from decay chain D2).

4.2 Parameter Fitting

In the previous subsection, we checked if it is possible to reconstruct the end points of invariant mass distributions involving charged leptons. Statistically, it seems possible to do so for decay modes D1) and D2). This constrains mass differences among \tilde{q}_L , $\tilde{\chi}_2^0$, $\tilde{\chi}_1^0$, \tilde{e}_R (D1) and \tilde{q}_L , $\tilde{\chi}_2^+$, $\tilde{\chi}_1^+$, $\tilde{\nu}_L$ (D2). We expect that these masses can be reconstructed with $O(10)$ GeV errors, as was the case in ref.[14]. However, the corresponding errors on some MSSM parameters are significantly larger.

In order to illustrate this point, we list two sets of MSSM parameters which reproduce all kinematic end points within $\Delta\chi^2 = 1$, where $\Delta\chi^2$ is defined as

$$\Delta\chi^2 = \sum_i (M_i^{\text{input}} - M_i^{\text{fit}})^2 / (\Delta M_i)^2. \quad (10)$$

Here M_i runs over all five end points, $m_{jl}^{\text{max}(\text{min})}$, $m_{jl}^{\text{max}(\text{min})}$ and m_{ll}^{max} , of the decay chains D1) and D2) listed in Table 3. We assume $\Delta(M_i)$ is 1% of M_i^{input} for distributions involving a jet, and 0.3 % of $m_{ll}^{\text{max,input}}$. In Table 4, we list the solution with maximal and minimal μ (for $\tan\beta \leq 20$) that satisfy $\Delta\chi^2 \leq 1$.

	$m_{\tilde{q}_L}$	M_1	M_2	μ	$\tan \beta$	$m_{\tilde{e}_R}$	$m_{\tilde{\nu}}$
μ max	575.381	108.279	196.758	235.711	20.0	147.366	202.577
μ min	554.638	99.578	218.696	180.096	20.0	135.18	185.826

Table 4: Maximal and minimal μ solution satisfying $\Delta\chi^2 \leq 1$

	$m_{\tilde{\chi}_1^0}$	$m_{\tilde{\chi}_2^0}$	$m_{\tilde{\chi}_3^0}$	$m_{\tilde{\chi}_4^0}$	$m_{\tilde{\chi}_1^+}$	$m_{\tilde{\chi}_2^+}$
μ max	101.79	163.15	244.85	284.94	160.44	285.10
μ min	89.0	150.97	190.41	268.72	144.19	268.74

Table 5: Neutralino and chargino masses in GeV for the maximal and minimal μ solution.

Note that the errors of the dimensionful parameters are strongly correlated, so that solutions with $\Delta\chi^2 < 1$ almost fall onto a one-dimensional line in the seven-dimensional parameter space. Table 4 shows that the kinematic quantities we have used in the fit give rather weak constraints for M_2 and μ , with errors of order 20 GeV to 50 GeV. In fact, for fixed $\tan \beta$ we find two distinct sets of solutions, with $\mu > M$ and $\mu < M$, respectively. Moreover, one cannot fix the actual value of $\tan \beta$ from this fit; one can only determine that $\tan \beta \gtrsim 8.65$ where the minimum is achieved when $M_2 \sim \mu$.

Table 5 shows that the corresponding chargino and neutralino masses only vary within 15 GeV between the two extreme solutions (except for $\tilde{\chi}_3^0$, which is almost not produced in \tilde{q} decays). Hence one will need additional information, beyond the kinematics of the decay chains D1) and D2), to reduce the errors on the fundamental parameters.

Reducing the errors on μ and $\tan \beta$ would be necessary to predict the thermal relic density accurately. The μ (max,min) solutions predict $\Omega_{\tilde{\chi}_1^0} h^2 = 0.160$ and 0.122 , respectively, as compared to 0.152 for the input point. The μ max point predicts a similar relic density as the input point; indeed, within the region with $\Delta\chi^2 \leq 1$, we were not able to find solutions with $\Omega_{\tilde{\chi}_1^0} h^2 > 0.165$. On the other hand, the μ min solution predicts a significantly smaller relic density, and even smaller values of $\Omega_{\tilde{\chi}_1^0} h^2$ are possible if we relax the upper bound on $\tan \beta$, which was imposed “by hand” in this fit. For example, there is a solution with $\tan \beta = 36$ and $(M_1, M_2, \mu, m_{\tilde{q}}, m_{\tilde{e}_R}, m_{\tilde{\nu}}) = (108.3, 194.7, 239.3, 576.9, 148.0, 203.9)$ (all masses in GeV), giving $\Omega_{\tilde{\chi}_1^0} h^2 = 0.112$. We hence need to reduce the errors on *both* μ and $\tan \beta$. The former determines the size of the higgsino components of the LSP, which begins to be significant in this region of parameter space. The product $\mu \tan \beta$ determines the amount of $\tilde{\tau}_L - \tilde{\tau}_R$ mixing, which reduces the predicted relic density through a reduced $\tilde{\tau}_1$ mass and enhanced S -wave annihilation. In the following we discuss strategies that might be useful for reducing the errors on these two quantities.

	$\tilde{\chi}_1^0$	$\tilde{\chi}_2^0$	$\tilde{\chi}_4^0$	$\tilde{\chi}_1^+$	$\tilde{\chi}_2^+$
μ max $\tilde{u}_L \rightarrow$	10^{-3}	0.257	0.073	0.553	0.113
$\tilde{d}_L \rightarrow$	0.036	0.214	0.094	0.412	0.238
μ min $\tilde{u}_L \rightarrow$	$0.4 \cdot 10^{-3}$	0.167	0.162	0.381	0.285
$\tilde{d}_L \rightarrow$	0.042	0.106	0.196	0.197	0.451

Table 6: Squark branching ratios for the maximal and minimal μ solutions.

	μ max	μ input(univ)	μ min
$\tilde{\chi}_2^0 \rightarrow \tilde{e}_R$	2×0.06	2×0.148	2×0.105
$\tilde{\chi}_2^+ \rightarrow \tilde{\nu}_e$	0.063	0.096	0.109
$\tilde{\nu}_e \rightarrow \tilde{\chi}_1^+$	0.433	0.402	0.380

Table 7: Branching ratios for the maximal and minimal μ solution. We assume universal soft sfermion masses and $A_\tau = 0$ at the weak scale.

One possibility is to measure some branching ratios. In Table 6, we compare the \tilde{q} decay branching ratios into charginos and neutralinos for the two solutions. Note that the ratio of the $\tilde{\chi}_2^+$ and $\tilde{\chi}_2^0$ modes increases by more than a factor of three, from 0.45 to 1.71 for \tilde{u}_L decay and from 1.11 to 4.25 for \tilde{d}_L decay, when switching from the μ max solution to the μ min solution. This is almost entirely due to the change of μ ; the value of $\tan\beta$ is not important here (as long as $\tan^2\beta \gg 1$).

The relative strengths of the signals from decay chains D1) and D2) should thus yield important information to reduce the errors on MSSM parameters. The strengths of these signals can be extracted purely kinematically, e.g. from the relative number of events with m_{ll} below the $\tilde{\chi}_2^0$ and $\tilde{\chi}_2^+$ edge, respectively, and/or by trying to determine the fraction of di-lepton events that have a τ -jet near the charged lepton pair, as discussed above. For a given solution in Table 4, all chargino and neutralino mixing angles and masses are fixed. As stated above, this is a fairly constrained fit where all relevant sparticle masses are effectively described by one parameter. The acceptances should then be very well calibrated from the mass constraints, so that systematic errors should be small.

In order to extract squark branching ratios from the number of events with a lepton pair in the final state, one must know $Br(\tilde{\chi}_2^0 \rightarrow \tilde{e}_R)$ and $Br(\tilde{\chi}_2^+ \rightarrow \tilde{\nu}_L)$. These branching ratios also depend on MSSM parameters, as shown in Table 7. Here we assume that the $\tilde{\tau}$ and $\tilde{\nu}_\tau$ soft breaking mass parameters are the same as for first and second generation sleptons. We compute the $\tilde{\tau}$ mixing angle by setting $A_\tau = 0$ at the weak scale; whenever it is sizable, $\tilde{\tau}_L - \tilde{\tau}_R$ mixing is anyway dominated by the contribution $\propto \mu \tan\beta$. With these assumptions all parameters required to compute these branching ratios can in principle be extracted from the kinematic fitting described above.

The least critical quantity in Table 7 is the branching ratio for $\tilde{\nu}_e \rightarrow \tilde{\chi}_1^+$ decays. It decreases slightly with decreasing μ , due to the shrinking wino component of $\tilde{\chi}_1^+$. However, this effect is weaker than the simultaneous increase of $Br(\tilde{\chi}_2^+ \rightarrow \tilde{\nu}_e)$, which is due to the increasing wino component of $\tilde{\chi}_2^+$. The strength of the signal from decay chain D2) is proportional to the product of these two branching ratios, which varies between 0.027 and 0.041. Together with the simultaneous change of $Br(\tilde{q}_L \rightarrow \tilde{\chi}_2^+)$ shown in Table 6, this means that for our choice of parameters the signal strength of D2) decreases rapidly with increasing μ . Moreover, the relevant branching ratios do not depend significantly on the details of the $\tilde{\tau}$ sector, and can thus be predicted fairly reliably from the quantities listed in Table 4.⁸

Unfortunately this is not true for the branching ratio for $\tilde{\chi}_2^0 \rightarrow \tilde{e}_R e$ decays, which does depend strongly on the mass and mixing angle of $\tilde{\tau}_1$. Note that the prediction in Table 7 for the input point (0.296) differs from the input value in Table 2 (0.236). This is because we ignored the reduction of soft breaking $\tilde{\tau}$ masses through RG effects when computing the

⁸In principle $\tilde{\chi}_2^+$ branching ratios could change somewhat if $m_{h_t} < m_{\tilde{\chi}_2^+} - m_{\tilde{\chi}_1^+}$, in which case additional 2-body decay modes of $\tilde{\chi}_2^+$ would open up. However, such scenarios are already tightly constrained by LEP data, and would give rise to a variety of Higgs signals at the LHC.

entries of Table 7. In the given case these effects only reduce $m_{\tilde{\tau}_1}$ by ~ 5 GeV. This is sufficient to increase the partial width for $\tilde{\chi}_2^0 \rightarrow \tilde{\tau}_1 \tau$ significantly; note that $\tilde{\chi}_2^0 \rightarrow \tilde{l} l$ decays are pure P-wave in the limit $m_l \rightarrow 0$, and the available phase space for these decays is not large in our case. Since for both fit solutions shown in Table 4 $\tan \beta$ is significantly larger than the input value, these solutions predict even lighter $\tilde{\tau}_1$ states and enhanced $\tilde{\tau}_L - \tilde{\tau}_R$ mixing. The use of these parameters would therefore underestimate the true branching ratio for $\tilde{\chi}_2^0 \rightarrow \tilde{e}_R e$ decays significantly.

In order to extract the squark branching ratios of Table 6 to better than a factor of 2 one will therefore need additional information on the $\tilde{\tau}$ sector. This might be obtained by studying $\tilde{\chi}_2^0 \rightarrow \tau^+ \tau^- \tilde{\chi}_1^0$ decays. As mentioned at the end of Sec. 3, it should be possible to determine the edge of the di- τ -jet invariant mass distribution to $\sim 5\%$. This would be sufficient to detect large differences between $\tilde{\tau}$ and \tilde{e} masses; however, it would not suffice to distinguish between the three cases used in Table 7. To this end one would need to determine the ratio of branching ratios for $\tilde{\chi}_2^0 \rightarrow e^+ e^- \tilde{\chi}_1^0$ and $\tilde{\chi}_2^0 \rightarrow \tau^+ \tau^- \tilde{\chi}_1^0$ decays. The precision of this measurement might be limited by systematic effects, since the two signals have very different efficiencies.⁹ However, given that this ratio of branching ratios differs by more than a factor of 4.5 between the three scenarios of Table 7 we think it likely that its measurement will help to reduce the errors of the extracted squark branching ratios significantly. Finally, once a linear collider of sufficient energy becomes available precision studies of $\tilde{\tau}_1$ production and decay will be possible [29, 30].

Let us summarize this somewhat complicated discussion by turning the argument around. One should first extract information about the $\tilde{\tau}$ sector, e.g. by comparing signals from $\tilde{\chi}_2^0 \rightarrow \tau^+ \tau^- \tilde{\chi}_1^0$ to those from $\tilde{\chi}_2^0 \rightarrow e^+ e^- \tilde{\chi}_1^0$. This will give information on the soft breaking masses in the $\tilde{\tau}$ sector as well as on the product $\mu \tan \beta$. This information, together with the result of the kinematic fit described above, will allow one to predict the branching ratios of the decays listed in Table 7 with reasonable precision. This in turn will allow to translate the measured strengths of the signals from decay chains D1) and D2) into squark branching ratios. Finally, these branching ratios can be used to greatly reduce the error on μ .

Another way to further constrain the relevant MSSM parameters is to include $\tilde{\chi}_4^0$ decay edges from decays D3) and D4) in the fit. Just measuring m_{ll}^{edge} values of these decay modes with 1% errors allows to reduce μ^{max} to 214 GeV. However, this would still not allow us to give an upper bound on $\tan \beta$.¹⁰ Moreover, this edge may not be visible for larger gluino and squark masses, where the production cross section is substantially smaller.

Given that the very weak upper bound $\tan \beta \leq 20$ which we imposed in the fit summarized in Table 4 is sufficient to predict $\Omega_{\tilde{\chi}_1^0}^{th} h^2 \simeq 0.135 \pm 0.03$, it seems certain that the strategy outlined above will again allow to predict the thermal relic density to better than 20%. The only loophole occurs if $\tan \beta$ is very large. In this case the $\tilde{\chi}_1^0 - \tilde{\tau}_1$ mass difference becomes so small that the τ from $\tilde{\tau}_1$ decays become effectively invisible at hadron colliders. At the same time $\tilde{\tau}_1 - \tilde{\chi}_1^0$ co-annihilation reduces the predicted LSP relic density by up to a factor of ten [35]. One would then need to increase m and/or M in order to get a cosmologically interesting value of $\Omega_{\tilde{\chi}_1^0} h^2$; $\tilde{\chi}_2^0 \rightarrow \tilde{e}_R e$ decays may not be open. In this case straightforward kinematic fitting as we described here will not be possible at the LHC, although one should still get a hint for the relative ordering of $\tilde{\tau}_1$ and \tilde{e}_R masses by observing τ -jets in missing E_T +jets events, which will yield the most robust SUSY signal in this case. In such a somewhat contrived scenario kinematical precision measurements would probably only be possible at a

⁹Since the $\tilde{\chi}_2^0 - \tilde{\tau}_1$ mass difference is quite small, one may have to allow one of the τ -jets to be quite soft.

¹⁰Including this new information gives the strong upper bound $\tan \beta \leq 11$ at the 1σ level, but $\tan \beta = 20$ remains allowed at 2σ .

lepton collider.

5 Discussion

In this paper, we argued that LHC experiments can play a substantial role in predicting the contribution $\Omega_{\tilde{\chi}_1^0}^{th}$ of thermal relic LSPs to the mass density of the Universe. Previous simulations in the literature were mostly done using mSUGRA assumptions, where usually $|\mu|^2 \gg M^2$. In such a case the measured $\tilde{\chi}_2^0$ cascade decay determines $m_{\tilde{e}_R}$, $m_{\tilde{\chi}_2^0}$ and $m_{\tilde{\chi}_1^0}$. Once we know that the LSP is mostly bino, these three masses are sufficient to determine $\Omega_{\tilde{\chi}_1^0}^{th}$ within 20%.

On the other hand, if Nature does not respect universality of all scalar soft breaking masses, it is possible that $\mu \sim M$. In such a case, one needs to know μ and M in addition to $m_{\tilde{\chi}_1^0}$ and $m_{\tilde{e}_R}$ to determine $\Omega_{\tilde{\chi}_1^0}^{th}$, because s -channel exchange of Z and h , or WW production might play important roles in $\tilde{\chi}_1^0$ pair annihilation in the early Universe. We showed that, if $\mu \sim M$, $\tilde{\chi}_2^+$ and $\tilde{\chi}_4^0$ will be produced copiously in \tilde{q}_L decays. One can then determine all MSSM parameters needed to predict $\Omega_{\tilde{\chi}_1^0}^{th}$ through the study of these cascade decay channels, using fits of kinematic end points and edges of invariant mass distributions. The isolation of $\tilde{\chi}_2^+ \rightarrow \tilde{\nu}_L \rightarrow \tilde{\chi}_1^+$ decays by observing the subsequent $\tilde{\chi}_1^+ \rightarrow \tilde{\tau}$ decay may be used to improve the reconstruction of the $\tilde{\chi}_2^+$ production and decay kinematics. Moreover, the measurement of the relative number of events from different decay chains further constrains MSSM parameters. In the end it should again be possible to predict the thermal LSP relic density with an error of 20% or better even in this more complicated scenario. In fact, this scenario is advantageous, since it allows us to determine both the gaugino and higgsino components of the LSP; these are needed to predict the strength of the LSP couplings to Higgs bosons, which in turn are required for predicting the LSP–nucleon scattering cross section. In mSUGRA scenarios with $|\mu| > M$ one can probably only establish an upper bound on the higgsino component of the LSP, which only allows one to derive upper bounds on LSP–Higgs couplings.

Notice that we *only* used information that can be extracted from studies at the LHC to arrive at this rather optimistic conclusion. If any one of the relevant masses could be determined with better precision elsewhere, e.g. at a lepton collider, the allowed region would shrink significantly, since the fit of hypothetical LHC data resulted in an almost one-dimensional $\Delta\chi^2 \leq 1$ domain.

In this paper we discussed the case where $m \ll M$ so that neutralino decay into sfermion is open. This is a good assumption if $\tilde{\chi}_1^0$ is gaugino like, as $\tilde{\chi}_1^0$ density overclose the Universe if $m \gg M$. For increased higgsino component of $\tilde{\chi}_1^0$, such a requirement is no longer necessary. It is interesting to see if one can extract sparticle masses from decay distributions for such cases.

In this paper, we did not study the case where $\mu \ll M_1, M_2$, where the higgsino-like states $\tilde{\chi}_1^0$, $\tilde{\chi}_2^0$ and $\tilde{\chi}_1^+$ are nearly degenerate in mass. In such a case we should observe $\tilde{\chi}_2^+$, $\tilde{\chi}_4^0$ production from squark decays in addition to $\tilde{\chi}_3^0$ production, which is now mostly \tilde{B} . If scalar masses are not too large so that decays of the heavier neutralinos and charginos into real sfermions are open, the analysis is similar to the one that has been given in Sec. 4. If the sfermion decay mode is closed, the decay to a (virtual) Higgs boson might play an important role, unlike the case where $\mu \sim M$. While on-shell Higgs bosons produced in SUSY cascade decays can be identified [24], the kinematical fitting would be more difficult since it would be entirely based on jets. Note, however, that the thermal relic density of higgsino-like LSPs is small unless $m_{\tilde{\chi}_1^0} \gtrsim 500$ GeV, in which case it might be difficult to even discover supersymmetry

at the LHC.

We also did not discuss the case where $M_2 \ll M_1, \mu$ suggested in models with anomaly mediated supersymmetry breaking [8]. These models predict a rather heavy gluino. This results in a limited number of events even at the LHC, making precision studies rather difficult. In models with a not too heavy gluino while keeping $M_2 \ll M_1, \mu$, the relative number of events from $\tilde{B} \rightarrow \tilde{e}_R$ and $\tilde{B} \rightarrow \tilde{e}_L$ might be useful to show that $M_1 \gg M_2$, if both modes are open. This would be sufficient to show that the thermal LSP relic density is small, independent of the relative ordering of M_2 and μ , since both wino-like and higgsino-like LSPs with mass in the (few) hundred GeV range annihilate efficiently.

We thus conclude that whenever LHC experiments find a large sample of SUSY events, it will be possible to either predict the thermal relic density of LSPs with a fairly small error, or else one will be able to conclude that thermal relic LSPs do not contribute significantly to the overall mass density of the Universe. In the latter case one would need physics beyond the MSSM, and/or a non-thermal LSP production mechanism, to explain the Dark Matter in the Universe.

Acknowledgements

The work of MD was supported in part by the “Sonderforschungsbereich 375–95 für Astro-Teilchenphysik” der Deutschen Forschungsgemeinschaft.

References

- [1] For a review, see H. E. Haber and G. L. Kane, Phys. Rep. **117**, 75 (1985).
- [2] E. Witten, Nucl. Phys. B**188**, 513 (1981).
- [3] C. Giunti, C.W. Kim and U.W. Lee, Mod. Phys. Lett. A**6**, 1745 (1991); U. Amaldi, W. de Boer and H. Fürstenau, Phys. Lett. B**260**, 447 (1991); P. Langacker and M. Luo, Phys. Rev. D**44**, 817 (1991); J. Ellis, S. Kelley and D.V. Nanopoulos, Phys. Lett. B**260**, 131 (1991).
- [4] For a review, see G. Jungman, M. Kamionkowski and K. Griest, Phys. Rep. **267**, 195 (1996).
- [5] Proceedings of the “1996 DPF/DPB Summer Study on High-Energy Physics”. Ed. D. G. Cassel, L. T. Gennari and R. H. Siemann.
- [6] DAMA Collaboration, Phys. Lett. B**480**, 23 (2000).
- [7] CDMS Collaboration, Nucl. Instrum. Meth. A**444**, 345 (2000).
- [8] T. Moroi and L. Randall, Nucl. Phys. B**570**, 455 (2000).
- [9] K. Enqvist and J. McDonald, Nucl. Phys. B**538**, 321 (1999).
- [10] G. F. Giudice, E. W. Kolb and A. Riotto, hep-ph/0005123.
- [11] K. Enqvist and J. McDonald, Phys. Rev. Lett.**83**, 2510 (1999).
- [12] M. S. Turner, astro-ph/9912211.

- [13] M. Brhlik, D.J.H. Chung and G.L. Kane, hep-ph/0005158.
- [14] H. Bachacou, I. Hinchliffe and F. E. Paige, Phys. Rev. **D62**, 015009 (2000).
- [15] J.R. Espinosa and R.-J. Zhang, hep-ph/9912236; M. Carena, H.E. Haber, S. Heinemeyer, W. Hollik, C.E.M. Wagner and G. Weiglein, hep-ph/0001002.
- [16] E. W. Kolb and M. S. Turner, *The Early Universe*, Addison-Wesley, 1990. K. Griest, M. Kamionkowski and M.S. Turner, Phys. Rev. **D41**, 3565 (1990).
- [17] K. Griest and D. Seckel, Phys. Rev. **D43** 3191 (1991).
- [18] S. Mizuta and M. Yamaguchi, Phys. Lett. **B298**, 120 (1993).
- [19] M. Drees and M. M. Nojiri, Phys. Rev. **D47**, 376 (1993).
- [20] M. Drees, M.M. Nojiri, D.P. Roy and Y. Yamada, Phys. Rev. **D56**, 276 (1997).
- [21] T. Falk, Phys. Lett. **B456**, 171 (1999).
- [22] M. Drees, and M. M. Nojiri, Nucl. Phys. **B369**, 54 (1992).
- [23] H. Baer, C.-H. Chen, M. Drees, F. Paige and X. Tata, Phys. Rev. Lett. **79**, 986 (1997).
- [24] ATLAS Collaboration, ATLAS Detector and Physics Performance Technical Design Report. CERN/LHCC99-19. <http://atlasinfo.cern.ch/Atlas/GROUPS/PHYSICS/TDR/access.html>
- [25] J.L. Feng, K.T. Matchev and F. Wilczek, Phys. Lett. **B482**, 388 (2000).
- [26] I. Hinchliffe, F. E. Paige, M. D. Shapiro, J. Soderqvist and W. Yao, Phys. Rev. D **55**, 5520 (1997).
- [27] M. M. Nojiri and Y. Yamada, Phys. Rev. **D60**, 015006 (1999).
- [28] I. Hinchliffe and F. E. Paige, Phys. Rev. **D61**, 095011 (2000).
- [29] M. M. Nojiri, Phys. Rev. **D51**, 6281 (1995).
- [30] M. M. Nojiri, K. Fujii, T. Tsukamoto, Phys. Rev. **D54**, 6756 (1996).
- [31] D. Pierce and A. Papadopoulos, Phys. Rev. **D50**, 565 (1994); Nucl. Phys. **B430**, 278 (1994); A .B. Lahanas, K. Tamvakis and N. D. Tracas, Phys. Lett. **B324**, 387 (1994).
- [32] F. E. Paige, S. D. Protopopescu, H. Baer and X. Tata, hep-ph/9810440.
- [33] E. Richter-Was et al., ATLFAST2.21, ATLAS Internal Note, PHYS-NO-079.
- [34] M. Drees, Y. G. Kim, M. M. Nojiri, D. Toya, K.Hasuko, and T. Kobayashi, work in progress.
- [35] J. Ellis, T. Falk, K. A. Olive and M. Srednicki, Astropart. Phys. **13**, 181 (2000).